Migration and infill of trenches in the marine environment : an analytical engineering model

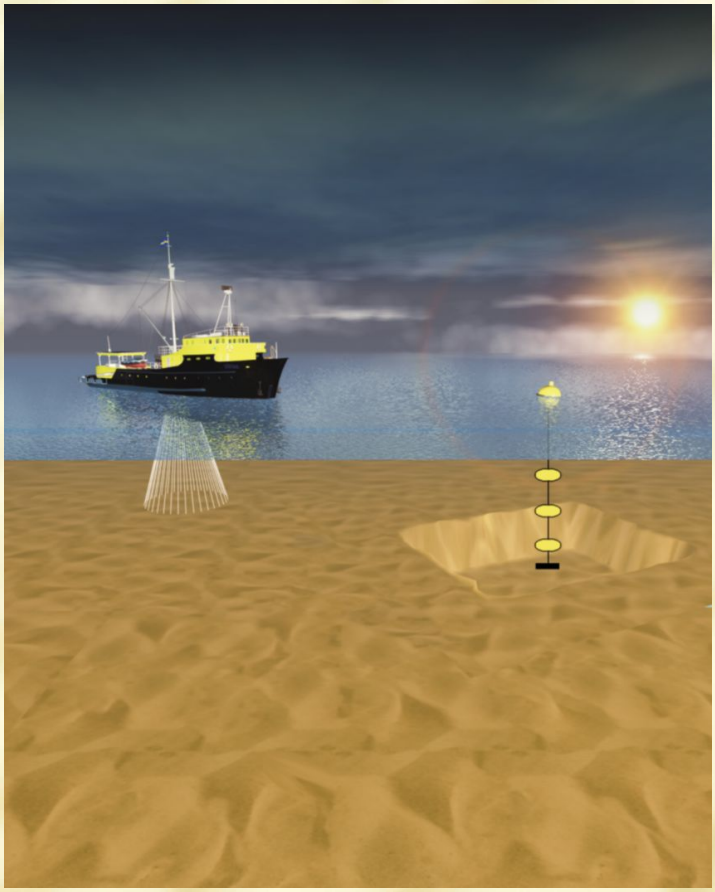

Jan S. Ribberink

University of Twente

November 2004

SANDPIT Fifth Framework Project No. EVK3-CT-2001-00056

University of Twente
The Netherlands

Migration and infill of trenches in the marine environment: an analytical engineering model

Jan S. Ribberink
November 2004

UNIVERSITY OF TWENTE

Contents

0 Introduction

Coastal seas experience an increasing pressure of human dredging activities for different purposes such as navigation (harbour access channels), communication cables, gas pipelines, sand mining. The present insights in the morphological consequences of sea bed dredging are still limited and there is a general need for adequate quantitative modelling tools of the involved morphodynamics.

In the present study an analytical model is developed for the description of the morphodynamics of dredged trenches in the marine environment. Large numerical model systems such as Delft2D/3D, Telemac, Mike21 are very useful for the simulation of the morphodynamics around specific realistic sand pit / trench designs, but their application is elaborate and time-consuming. Consequently these systems are also less useful for developing insight in the parameters controlling morphodynamic behaviour and how this behaviour can be influenced.
Recently Roos (2004) developed a semi-analytical linear model for sand pits of different shapes in the sea and provided new insights in 2DH morphodynamic processes, occurring in and around pits and interacting with natural sea bed morphodynamics (tidal sand banks) .

In the present study a simple engineering model is developed for (dredged) trenches in the marine environment. Using simplified 1D flow and sediment transport schematisations, an harmonic analysis is carried out to obtain insights in

i) the process parameters, controlling the morphological behaviour of trenches under the influence of short surface waves and mean currents, and
ii) how this behaviour is affected by the geometry (length and depth) of trenches.

Simple analytical expressions are derived for the *migration velocity* and *infill time* of trenches as a function of the local wave / current and sediment conditions and of the trench dimensions (length and depth). The analytical expressions are verified with numerical model simulations of trench cases in different parameter regimes using the model LOMOR (Ribberink and Buijsrogge, 2003; see Appendix E).

The research is carried out at the University of Twente in the framework of the EU project Sandpit (Fifth Framework Project No. EVK3-CT-2001-00056) and is partly funded by this project.

1 Basic equations

Trenches or channels are considered with their main axis normal to the direction of a steady current. The surrounding sea bed is assumed to be horizontal. In this way the morphological development of the trench is treated as a one-dimensional problem (x-direction is flow direction).

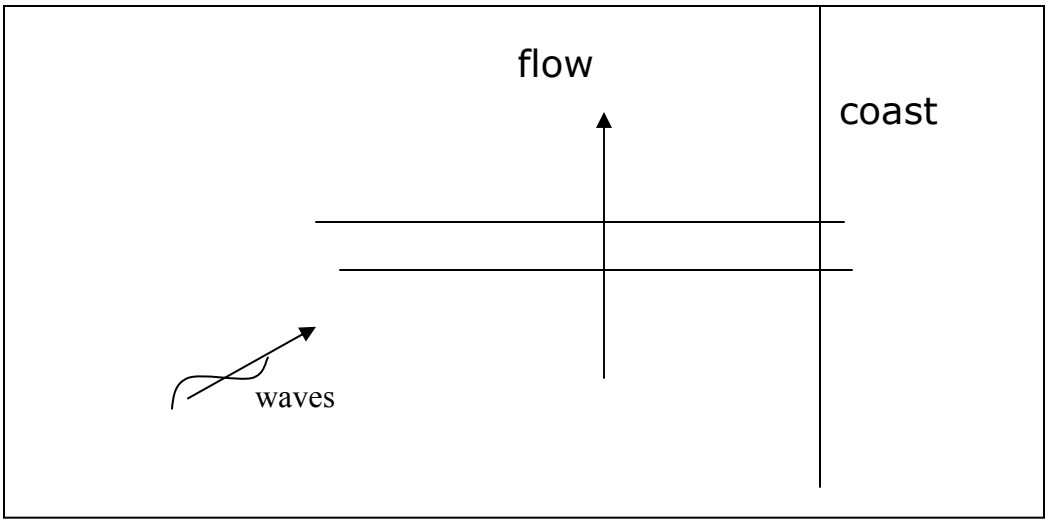

Figure 1 Trenches or channels normal to a steady current

Flow

The one-dimensional shallow-water flow equations for depth-averaged flow are:

(1)

$$\frac{\partial u}{\partial t} + u\frac{\partial u}{\partial x} + g\frac{\partial z_b}{\partial x} + g\frac{\partial h}{\partial x} = R$$

$$\frac{\partial h}{\partial t} + \frac{\partial uh}{\partial x} = 0$$

with:
u = depth averaged flow velocity
h = water depth
z_b = bed level
R = friction term

It can be shown that for tidal flows over channels with length L , depth h (of the same order of magnitude as the water depth) and flow velocities of order u, the relative order of magnitude of the terms in (1) is:

$\frac{L}{gh}\frac{u}{T}$ (acceleration): $\frac{u^2}{gh}$ (advection) : 1 (bed-level gradient) : 1 (water-level gradient) : $\frac{u^2}{gh}.\frac{Lg}{C^2h}$ (friction)

In the marine environment with tidal periods T=12.5 h, depths h=10-30 m, velocities u=0-2 m/s, the Froude number $Fr = u/\sqrt{gh} << 1$. Assuming trenches with lengths 1-100 times the water depth (L/h=1-100) and Chezy values C=40-80 $m^{1/2}$ /s, the acceleration, advection and friction term are generally of much smaller magnitude than the bed- and water level gradient terms.

The equations can now be simplified to :

(2)

$$\frac{\partial z_b}{\partial x} + \frac{\partial h}{\partial x} = 0$$

$$\frac{\partial uh}{\partial x} = \frac{\partial q}{\partial x} = 0$$

with q is the water discharge per unit width.

Waves

Short wave characteristics wave height H and wave period T are assumed to be spatially constant and are not affected by the trench. Linear wave theory is assumed to be valid for the description of the near-bed wave orbital flow:

(3)

$$\hat{U} = \pi \frac{H}{T} \frac{1}{\sinh(k_w h)}$$

with:

k_w = wave number

h = water depth

and the dispersion relation:

(4) $$k_{w_\infty} h = k_w h.\tanh(k_w h)$$

with:

$$k_{w_\infty} = \frac{2\pi}{L_\infty} = \frac{4\pi^2}{gT^2}$$ = ‘ deep water’ wave number

Sediment transport

The sediment transport is divided in a bed-load and a suspended-load part (q_b and q_s), using a time-averaged formulation over the wave period. Only the current-related transport components are used, assuming that the wave–related components are generally only dominant in cross-shore direction, i.e. perpendicular to the mean flow direction.

The bed-load transport is written as a function of local hydrodynamic parameters and of other constant parameters (e.g. sediment grain size and bed roughness) in the following general form:

(5)

$$q_b = f_1(u, \hat{U}, i_b, parameters)$$

with i_b is the local bed slope , $i_b = \partial z_b / \partial x$.

Suspended sediment concentrations are described with the depth-averaged formulation of Galappatti, based on an asymptotic solution of the 3D advection-diffusion equation (see Galappatti and Vreugdenhil, 1985). In one-dimensional form:

$$T_A \frac{\partial \overline{C}}{\partial t} + L_A \frac{\partial \overline{C}}{\partial x} = \overline{C_e} - \overline{C}$$

With:

$\overline{C}$ = depth-averaged sediment concentration

T_A = adjustment time of suspended sediment ($= \widetilde{T}.h/W_s$, with $\widetilde{T}_s < 1$)

L_A = adjustment length of suspended sediment ($= \widetilde{L}u.h/W_s$, with $\widetilde{L} < 1$)

$\overline{C_e}$ = depth-averaged equilibrium sediment concentration

W_s = settling velocity of sediment

For tidal flow, sandy beds and trench lenght scales of 10-100 times the water depth the time –derivative term is generally negligible, and only spatial lag effects are important :

(6)

$$L_A \frac{\partial \overline{C}}{\partial x} = \overline{C_e} - \overline{C}$$

The adjustment length can be written as:
(6a)

$$L_A = \tilde{L}.\frac{u.h}{W_s}$$

With $\tilde{L}$ is a coefficient, depending on the shape of the vertical concentration distribution ($0.1 < \tilde{L} < 1$) . It is treated here as a constant which has to be selected in advance (standard value $\tilde{L}$ =0.5)
The equilibrium concentration is written as a function of local hydrodynamic and sediment parameters in the following general form:

(7)

$$\overline{C}_e = f_2(u, \hat{U}, i_b, parameters)$$

The suspended sediment transport can now be calculated from :

(8) $$q_s = \alpha_s u h \overline{C}$$

with α_s is profile shape coefficient.

Bed-level changes
The bed-level changes are calculated with the sediment continuity equation :

(9)

$$\frac{\partial z_b}{\partial t} + \frac{1}{1-\varepsilon_0}\frac{\partial (q_b + q_s)}{\partial x} = 0$$

with:

ε_0 = porosity (=0.4)

2 Morphodynamic model

Substituting (8) and (5) in (9) gives:

(10)

$$(1-\varepsilon_0)\frac{\partial z_b}{\partial t} + f'_{1_u}\frac{\partial u}{\partial x} + f'_{1_{\hat{U}}}\frac{\partial \hat{U}}{\partial x} + f'_{1_{i_b}}\frac{\partial i_b}{\partial x} + \alpha_s q\frac{\partial \overline{C}}{\partial x} = 0$$

u can be expressed in z_b using (2) as follows:

(11)

$$\frac{\partial u}{\partial x} = -\frac{u}{h}\frac{\partial h}{\partial x} = \frac{u}{h}\frac{\partial z_b}{\partial x}$$

$\hat{U}$ can be also be expressed in z_b trough its dependence of $k_{w0}h$ ((3) and (4)) and using the fact that the 'deep water' wave number $k_{w_\infty} = \frac{2\pi}{L_0} = \frac{4\pi^2}{gT^2}$ is constant in space:

(12)

$$\frac{\partial \hat{U}}{\partial x} = \frac{\partial \hat{U}}{\partial k_w h}.\frac{\partial k_w h}{\partial k_{w_\infty} h}.\frac{\partial k_{w_\infty} h}{\partial x} = f_3.k_{w_\infty}\frac{\partial h}{\partial x} = -f_3.k_{w_\infty}\frac{\partial z_b}{\partial x}$$

with (see Appendix A):

(13)

$$f_3 = -\frac{\pi H}{T}\frac{\cosh k_w h}{(k_w h + \sinh(k_w h)\cosh(k_w h)).\tanh^2 k_w h}$$

Since $i_b = \frac{\partial z_b}{\partial x}$:

(14)

$$\frac{\partial i_b}{\partial x} = \frac{\partial^2 z_b}{\partial x^2}$$

Substitution of (11), (12) and (14) in (10) gives:

(15)

$$(1-\varepsilon_0)\frac{\partial z_b}{\partial t} + f'_{1_u}\frac{u}{h}\frac{\partial z_b}{\partial x} - f'_{1_{\hat{U}}} f_3 . k_{w_\infty}\frac{\partial z_b}{\partial x} + f'_{1_{i_b}}\frac{\partial^2 z_b}{\partial x^2} + \alpha_s q\frac{\partial \overline{C}}{\partial x} = 0$$

The equations are now linearized around a basic sea-bed state, representing the 'undisturbed' conditions upstream and far downstream of the trench, consisting of a horizontal sea bed with constant uniform flow conditions (current and waves) and suspended sediment concentrations in equilibrium:

(16)

$u = u_0$
$h = h_0$
$\hat{U} = \hat{U}_0$
$z_b = z_{b0} = 0$
$i_b = i_{b0} = 0$
$\overline{C} = \overline{C_{e_0}}$

Assuming small sea-bed level variations z_b with respect to the water depth, (15) can be linearized as follows:

(17)

$$(1-\varepsilon_0)\frac{\partial z_b}{\partial t} + [f'_{1_u}]_0\frac{u_0}{h_0}\frac{\partial z_b}{\partial x} - [f'_{1_{\hat{U}}}]_0 . [f_3]_0 . k_{w_\infty}\frac{\partial z_b}{\partial x} + [f'_{1_{i_b}}]_0\frac{\partial^2 z_b}{\partial x^2} + \alpha_s q\frac{\partial \overline{C}}{\partial x} = 0$$

in which index '0' in the coefficients of the spatial derivatives refers to the basic state.

Subsituting (6) into (17) and taking the derivative to x gives:

(18)

$$(1-\varepsilon_0)\frac{\partial^2 z_b}{\partial x \partial t} + [f'_{1_u}]_0\frac{u_0}{h_0}\frac{\partial^2 z_b}{\partial x^2} - [f'_{1_{\hat{U}}}]_0 . [f_3]_0 . k_{w_\infty}\frac{\partial^2 z_b}{\partial x^2} + [f'_{1_{i_b}}]_0\frac{\partial^3 z_b}{\partial x^3} + \frac{\alpha_s q}{L_A}\frac{\partial \overline{C}_e}{\partial x} - \frac{\alpha_s q}{L_A}\frac{\partial \overline{C}}{\partial x} = 0$$

Since the equilibrium concentration also depends on the local flow /bed conditions (see (7)), its spatial derivative can be written in terms of spatial derivatives of bed level z_b, similar as was done for the bed-load transport:

(19)

$$\frac{\partial \overline{C}_e}{\partial x} = f_2{}'_u . \frac{u}{h} \frac{\partial z_b}{\partial x} - f_2{}'_{\hat{U}} f_3 . k_{w_\infty} \frac{\partial z_b}{\partial x} + f_2{}'_{i_b} \frac{\partial^2 z_b}{\partial x^2}$$

Substituting the linearized form of (19) into (18) gives:

(20)

$$(1-\varepsilon_0)\frac{\partial^2 z_b}{\partial x \partial t} + \mathrm{X}_1 \frac{\partial^2 z_b}{\partial x^2} + [f_1{}'_{i_b}]_0 \frac{\partial^3 z_b}{\partial x^3} + \frac{\alpha_s q}{L_A} \mathrm{X}_2 \frac{\partial z_b}{\partial x} + \frac{\alpha_s q}{L_A} [f_2{}'_{i_b}]_0 \frac{\partial^2 z_b}{\partial x^2} - \frac{\alpha_s q}{L_A} \frac{\partial \overline{C}}{\partial x} = 0$$

with:

(21)

$$\mathrm{X}_1 = \frac{u_0}{h_0}[f_1{}'_u]_0 - [f_3]_0 k_{w_\infty} [f_1{}'_{\hat{U}}]_0$$

$$\mathrm{X}_2 = \frac{u_0}{h_0}[f_2{}'_u]_0 - [f_3]_0 k_{w_\infty} [f_2{}'_{\hat{U}}]_0$$

Elimination of $\partial \overline{C} / \partial x$ from (20) using (17) finally leads to:

(22)

$$\frac{\partial z_b}{\partial t} + c \frac{\partial z_b}{\partial x} + D \frac{\partial^2 z_b}{\partial x^2} + L_A \frac{\partial^2 z_b}{\partial x \partial t} + P \frac{\partial^3 z_b}{\partial x^3} = 0$$

with advection due to bed-load as well as suspended-load:

(23)
$$c = c_b + c_s = \frac{\mathrm{X}_1}{(1-\varepsilon_0)} + \frac{\alpha_s q \mathrm{X}_2}{(1-\varepsilon_0)}$$

$c_b =$ migration velocity due to bed-load

$c_s =$ migration velocity due to suspended load

with diffusion due to bed-slope effects as well as due to suspension lag-effects:

(24)
$$D = L_A . c_b + D_{ib} + D_{is} = L_A . \frac{\mathrm{X}_1}{1-\varepsilon_0} + \frac{[f_1{}'_{i_b}]_0}{1-\varepsilon_0} + \frac{\alpha_s q [f_2{}'_{i_b}]_0}{1-\varepsilon_0}$$

D_{i_b} = diffusion coefficient due to bed-slope effect on bed-load

D_{i_s} = diffusion coefficient due to bed-slope effect on suspended-load

(25) $$P = L_A . D_{ib} = L_A . \frac{[f_1{}'_{i_b}]_0}{(1-\varepsilon_0)}$$

(26) $$L_A = \tilde{L}\frac{q}{W_s}$$ =adjustment length for suspended sediment

The model can also be written as:

(27)

$$\frac{\partial z_b}{\partial t} + c\frac{\partial z_b}{\partial x} + (D_{i_b} + D_{i_s})\frac{\partial^2 z_b}{\partial x^2} + L_A \frac{\partial}{\partial x}\{\frac{\partial z_b}{\partial t} + c_b \frac{\partial z_b}{\partial x} + D_{i_b}\frac{\partial^2 z_b}{\partial x^2}\} = 0$$

Two advection-diffusion processes are coupled in this equation through a first-order spatial adjustment process (adjustment length=L_A). Two extreme cases can be distinguished:

1. Suspension is in equilibrium and controlled by local conditions (L_A->0)
   Equation (27) reduces to an advection diffusion equation with migration velocity c (bed-load + suspended load) and diffusion coefficient D_i (damping due to bed-slope effect). The suspended-load contributes to the morphodynamics in the same way as bed-load.

2. Suspension is behaving as wash-load and controlled by the influx at the upstream boundary (L_A->∞)
   Equation (27) reduces to an advection diffusion equation with migration velocity c_b (only bed-load) and diffusion D_{ib} (damping due to bed-slope effect of bed-load). The suspended-load does not contribute to the morphodynamics.

3 Wave migration and amplitude decay

3.1 General

For sinusoidal bed-waves with wave length L (=2π/k, k=wave number) and wave period T(=2π/ω, ω=angular frequency):

(28) $$z' = \Delta z e^{i(kx-\omega t)} + \text{ c.c.}$$

Substituting (28) into (22) leads to :

$$-i\omega + cik - Dk^2 + L_A \omega k - D_{i_b} L_A i k^3 = 0$$

which can be written as a ω-k relation as follows:

(29) $$\omega = \frac{L_A k^3 (c_b L_A + D_{i_s}) + ck}{L_A^2 k^2 + 1} + i.k^2 \frac{-c_s L_A + D_{i_s} + D_{i_b}(L_A^2 k^2 + 1)}{L_A^2 k^2 + 1} = \omega_r + i\omega_i$$

which shows that ω consists of a real part (=ω_r) and an imaginary part (= ω_i). Substituting this into (28) gives:

(30) $$z' = \Delta z e^{\omega_i t} e^{i(kx-\omega_r t)}$$

or in terms of migration velocity c_{bed} and amplitude decay time T_{bed}:

(31) $$z' = \Delta z e^{-\frac{t}{T_{bed}}} e^{ik(x-c_{bed}t)}$$

with:

(32) $$c_{bed} = \frac{\omega_r}{k} = c_b + \frac{c_s + L_A k^2 D_{i_s}}{L_A^2 k^2 + 1}$$

(33) $$T_{bed} = -\frac{1}{\omega_i} = \left\{ \frac{k^2 (c_s L_A - D_{i_s})}{L_A{}^2 k^2 + 1} - D_{i_b} k^2 \right\}^{-1}$$

Remarks:

- In case of only bed-load or suspension with very long adjustment lenghts $L_A k >> 1$:

  $c_{bed} = c_b$ and $T_{bed} = -\frac{1}{D_{i_b} k^2}$

  Suspended-load does not contribute to the morphodynamics, and amplitude decay is especially quick for small bed wave-lenghts ($k \to \infty$).

- In case of no bed-load (c_b=0) and no bed-slope effect (D_i=0) :

  $c_{bed} = c_s/(L_A{}^2 k^2+1)$ and $T_{bed} = (L_A{}^2 k^2+1)/c_s L_A k^2 = 1/(c_{bed} L_A k^2)$

  If the flow changes sign : $c_{bed}<0$, but also $L_A<0$, so always resulting in a positive amplitude decay time (or still a negative growth rate , or stability).

In principle, the equations (32) and (33) can be used to estimate the migration velocity and amplitude decay time of bed waves with any length L (or wave number), once the basic state (horizontal bed) is known (water depth h_0, flow velocity u_0, wave height H and wave period T, sediment settling velocity W_s, Chezy bed roughness).

In the following section the expressions are worked out further for the power-law type transport formula of Bailard (1981).

3.2 The power-law transport formula of Bailard (1981)

The energetics-type transportformula of Bailard (1981) consists of a separate bed-load transport and a suspended-load transport power-law description of the intra-wave time-dependent near-bed velocity, resulting from the combined wave-current water motion.

The bed-load formula can be written as:

(34)

$$\vec{q}_b = m_b u_b^2 \vec{u}_b - m_b \frac{\vec{i}_b}{\tan\varphi} \left| u_b^3 \right|$$

in which:

(34a)

u_b = time-dependent near-bed flow velocity due to waves and the steady current

$m_b = \frac{c_f \varepsilon_b}{\Delta g \tan\varphi}$

ε_b= efficiency factor (=0.1)

c_f =friction factor

Δ = relative density of sediment (=1.65)
φ = angle of repose of the sediment

Assuming sinusoidal waves propagating in a direction normal to a mean current u x-direction and only accounting for the stirring effect of waves (current-dominated conditons), the wave-averaged bed-load load component in this x-direction (current-related transport) can be approximated as follows (see Appendix B):

(35) $$q_b = f_1 = m_b\left[\ \alpha_b^3 u^3 + \frac{1}{2}\alpha_b u\hat{U}^2\ \right] - m_b \frac{\partial z_b/\partial x}{\tan\varphi}.P$$

with:

(35a) for $\alpha_b^2 u^2 > \tilde{U}^2$: $$P = \left\{\alpha_b^3\left|u^3\right| + \frac{3}{4}\alpha_b\hat{U}^2|u|\right\}$$ current dominant

(35b) for $\tilde{U}^2 > \alpha_b^2 u^2$: $$P = \left\{\frac{4}{3\pi}\hat{U}^3 + \frac{3}{\pi}\alpha_b^2 u^2\hat{U}\right\}$$ wave dominant

The suspended sediment transport is described in a similar power-law shape. Using a power 4, as proposed by Bailard (1981), and neglecting bed-slope effects the wave- and depth-averaged equilibrium sediment concentration can be written as (see Appendix B):

(36a) for $\alpha_b^2 u^2 > \tilde{U}^2$: $$\overline{C}_e = f_2 = \frac{m_s}{|q|}\left\{\alpha_s^3 u^4 + \frac{3}{4}\alpha_s\hat{U}^2u^2\right\}$$ current dominant

(36b) for $\tilde{U}^2 > \alpha_b^2 u^2$: $$\overline{C}_e = f_2 = \frac{m_s}{|q|}\left\{\frac{4}{3\pi}\hat{U}^3|u| + \frac{3}{\pi}\alpha_s^2\left|u^3\right|\hat{U}\right\}$$ wave dominant

with:

(36c)
$$m_s = \frac{\varepsilon_s c_f}{\Delta g W_s}$$
ε_s= efficiency factor (=0.02)

The function f_3 (13) was derived in Appendix A:

(37)
$$f_3 = -\frac{\pi H}{T}\frac{\cosh k_w h}{(k_w h + \sinh(k_w h)\cosh(k_w h)).\tanh^2 k_w h}$$

The equations (35), (36) and (37) can now be used to work out expressions for the migration velocities c_b and c_s and for the diffusion coefficients D_{i_b} and D_{i_s} ((23), (24) with (21)) for the basic state '0' (see Appendix C):

(38) $$c_b = \frac{1}{(1-\varepsilon_0)h}[3q^c_{b_0} + q^{wc}_{b_0}(1+2f)]$$ current and wave dominant

with:

(38a) $$q^c_{b_0} = m_b \alpha_b^3 u_0^3$$

(38b) $$q^{wc}_{b_0} = \frac{1}{2} m_b \alpha_b \hat{U}_0^2 u_0$$

(38c) $$f = \frac{k_{w_\infty} h_0 . \sinh(2k_{w_0} h_0)}{(2k_{w_0} h_0 + \sinh(2k_{w_0} h_0)) . \tanh^2(k_{w_0} h_0)}$$

(39) $$c_s = \frac{1}{(1-\varepsilon_0)h}[4q^c_{s_0} + 2q^{wc}_{s_0}(1+f)]$$ current dominant

$$c_s = \frac{1}{(1-\varepsilon_0)h}[q^w_{s_0}(1+3f) + \alpha_s q^{cw}_{s_0}(3+f)]$$ wave dominant

with:

(39a) $$q^c_{s_0} = m_s \alpha_s^4 u_0^4 \frac{q}{|q|}$$ current dominant

(39b) $$q^{wc}_{s_0} = \frac{3}{4} m_s \alpha_s^2 \hat{U}_0^2 u_0^2 \frac{q}{|q|}$$

(39c) $$q^w_{s_0} = m_s \frac{4}{3\pi} \hat{U}_0^3 \alpha_s u_0$$ wave dominant

(39d) $$q^{cw}_{s_0} = \frac{3}{\pi} m_s \alpha_s^2 \hat{U}_0 u_0^3$$

(40) $$D_{i_b} = -\frac{\left|q^c_{b_0}\right| + \frac{3}{2}\left|q^{wc}_{b_0}\right|}{(1-\varepsilon_0)\tan\varphi}$$ current dominant

$$D_{i_b} = -\frac{q_b^w + \frac{3}{2} q_b^{cw}}{(1-\varepsilon_0)\tan\varphi} \qquad \text{wave dominant}$$

$$D_{i_s} = 0 \qquad \text{current and wave dominant}$$

with:

(40a) $$q_{b_0}^w = m_b \frac{4}{3\pi} \hat{U}^3 \qquad \text{wave dominant}$$

(40b) $$q_{b_0}^{cw} = \frac{2}{\pi} m_b \alpha_b^2 \hat{U}_0 u_0^2$$

Additional contributions of the waves are indicated with the superscripts $..^{wc}$ or $..^{cw}$. Superscript $..^{c}$ refers to the situation of only steady current (no waves). The subscript $..{}_0$ refers to the basic state.

Substitution of (38)…(40) into (32) and (33) leads to:

(41a) $$c_{bed} = \frac{1}{(1-\varepsilon_0)h_0}\left\{3q_{b_0}^c + q_{b_0}^{wc}(1+2f) + \frac{4q_{s_0}^c + 2q_{s_0}^{cw}(1+f)}{L_A^2 k^2 + 1}\right\} \quad \text{current dominant}$$

$$c_{bed} = \frac{1}{(1-\varepsilon_0)h_0}\left\{3q_{b_0}^c + q_{b_0}^{wc}(1+2f) + \frac{q_{s_0}^w(1+3f) + \alpha_s q_{s_0}^{cw}(3+f)}{L_A^2 k^2 + 1}\right\} \quad \text{wave dominant}$$

(41b) $$T_{bed} = (1-\varepsilon_0)h_0\left\{L_A k^2 \frac{\left[4q_{s_0}^c + 2q_{s_0}^{wc}(1+f)\right]}{L_A^2 k^2 + 1} + \frac{k^2 h}{\tan\varphi}\left[\left|q_{b_0}^c\right| + \frac{3}{2}\left|q_{b_0}^{wc}\right|\right]\right\}^{-1} \quad \text{current dom}$$

$$T_{bed} = (1-\varepsilon_0)h_0\left\{L_A k^2 \frac{\left[q_{s_0}^w(1+3f) + \alpha_s q_{s_0}^{cw}(3+f)\right]}{L_A^2 k^2 + 1} + \frac{k^2 h}{\tan\varphi}\left[q_b^w + \frac{3}{2} q_b^{cw}\right]\right\}^{-1} \quad \text{wave dom}$$

In order to study the influence of suspended sediment and of waves on the morphological behaviour, the migration velocity and amplitude decay time are studied relative to the situation for bed-load and a steady current alone (no waves). A non-dimensional

migration velocity $\widetilde{c}_{bed}$ and damping time $\widetilde{T}_{bed}$ are defined, using the migration velocity for only bed-load and and a steady current (no waves). In that case the migration velocity is equal to the well-known morphological characteristic velocity as derived by de Vries (see Jansen et al., 1994) :

$$c_b^c = \frac{3q_{b_0}^c}{(1-\varepsilon_0)h} \tag{42}$$

So, a non-dimensional migration velocity follows from dividing (41a) by (42):

$$\widetilde{c}_{bed} = \frac{c_{bed}}{c_b^c} \tag{43}$$

And a non-dimensional amplitude decay time follows from dividing (41b) by $\left|c_b^c\right| / h$ (= time needed for migration over a length equal to the water depth h in case of bed-load and a current alone):

$$\widetilde{T}_{bed} = T_{bed} . \left|c_b^c\right| / h \tag{44}$$

Finally, substitution of (32), (38)…(42) into (43) resp. (44) gives:

$$\widetilde{c}_{bed} = 1 + \frac{1}{3}\frac{q_{b_0}^{wc}}{q_{b_0}^c}(1+2f) + \frac{1}{3}\frac{4\dfrac{q_{s_0}^c}{q_{b_0}^c} + 2\dfrac{q_{s_0}^{wc}}{q_{b_0}^c}(1+f)}{L_A^2 k^2 + 1} \qquad \text{current dominant} \tag{45}$$

$$\widetilde{c}_{bed} = 1 + \frac{1}{3}\frac{q_{b_0}^{wc}}{q_{b_0}^c}(1+2f) + \frac{1}{3}\frac{\dfrac{q_{s_0}^w}{q_{b_0}^c}(1+3f) + \alpha_s \dfrac{q_{s_0}^{cw}}{q_{b_0}^c}(1+f)}{L_A^2 k^2 + 1} \qquad \text{wave dominant}$$

(46) $$\widetilde{T}_{bed} = \left\{ \frac{1}{3} kh.L_A k \frac{\left[4 \frac{q^c_{s_0}}{\left|q^c_{b_0}\right|} + 2 \frac{q^{wc}_{s_0}}{\left|q^c_{b_0}\right|}(1+f) \right]}{L_A^2 k^2 + 1} + \frac{1}{3} \frac{(kh)^2}{\tan\varphi} \left[1 + \frac{3}{2} \frac{\left|q^{wc}_{b_0}\right|}{\left|q^c_{b_0}\right|} \right] \right\}^{-1}$$ current dom

$$\widetilde{T}_{bed} = \left\{ \frac{1}{3} kh.L_A k \frac{\left[\frac{q^w_{s_0}}{\left|q^c_{b_0}\right|}(1+3f) + \alpha_s \frac{q^{cw}_{s_0}}{\left|q^c_{b_0}\right|}(3+f) \right]}{L_A^2 k^2 + 1} + \frac{1}{3} \frac{(kh)^2}{\tan\varphi} \left[\frac{q^w_{b_0}}{\left|q^c_{b_0}\right|} + \frac{3}{2} \frac{q^{cw}_{b_0}}{\left|q^c_{b_0}\right|} \right] \right\}^{-1}$$ wave dom

The contributions of suspended load and waves to the migration velocity and amplitude decay time can be distinguished in these expressions through the various sub- and superscript symbols.

4 Steady current, no waves

For the situation that only a current and no waves are present the following relations result from (41):

$$(47a)\qquad c_{bed} = \frac{1}{(1-\varepsilon_0)h_0}\left\{3q_{b_0}^c + \frac{4q_{s_0}^c}{L_A^2k^2+1}\right\}$$

$$(47b)\qquad T_{bed} = (1-\varepsilon_0)h_0\left\{L_Ak^2\,\frac{4\left|\,q_{s_0}^c\,\right|}{L_A^2k^2+1} + \frac{k^2h_0}{\tan\varphi}\left|q_{b_0}^c\right|\right\}^{-1}$$

The non-dimensional expressions become:

$$(48a)\qquad \widetilde{c}_{bed} = 1 + \frac{\frac{4}{3}\frac{q_{s_0}^c}{q_{b_0}^c}}{L_A^2k^2+1}$$

$$(48b)\qquad \widetilde{T}_{bed} = \left\{\frac{1}{3}\frac{h_0}{L_A}(L_Ak)^2\,\frac{\left[4\dfrac{q_{s_0}^c}{\left|q_{b_0}^c\right|}\right]}{L_A^2k^2+1} + \frac{1}{3}\left(\frac{h_0}{L_A}\right)^2\frac{(L_Ak)^2}{\tan\varphi}\right\}^{-1}$$

The relations are depicted in the Figures 1 and 2.

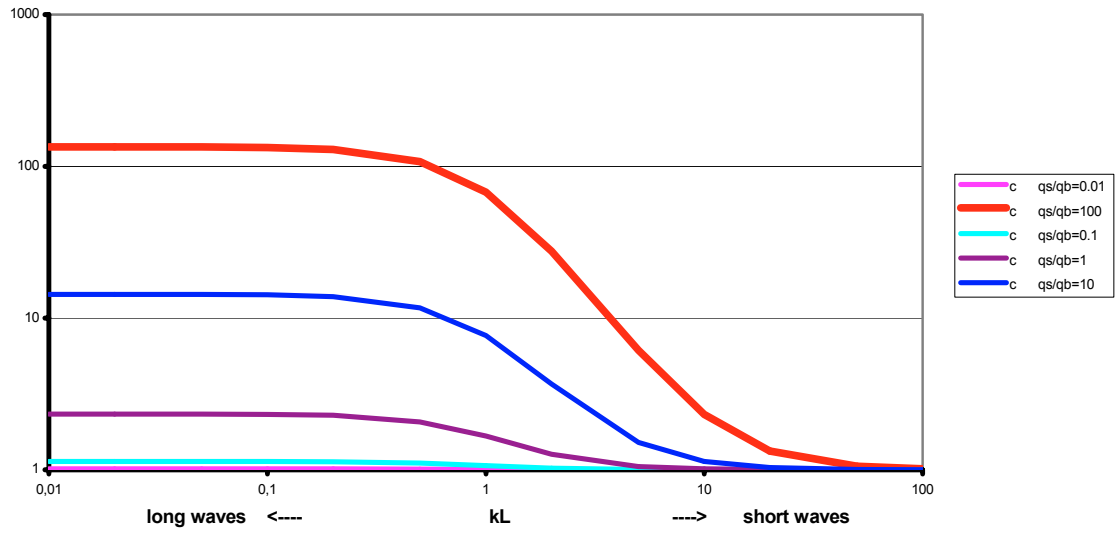

Figure 1 Non-dimensional migration velocity $\widetilde{c}_{bed}$ of bed waves as a function of kL_A (= ratio of suspension adjustment length and bed wave length) for different suspended-load /bed-load transport ratio's q_s/q_b.

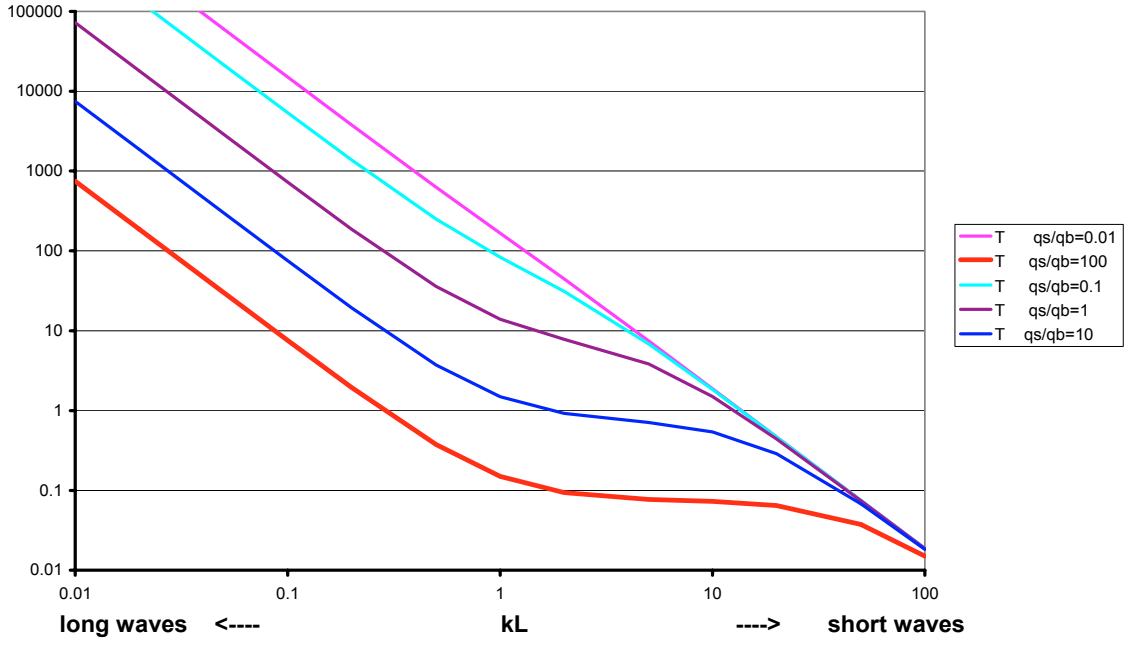

Figure 2 Non-dimensional amplitude-decay time $\widetilde{T}_{bed}$ as a function of kL_A (= ratio of suspension adjustment length and bed wave length) for different suspended-load/ bed-load transport ratio's q_s/q_b (h_0/L_A=0.1, $\varphi=32^0$).

The Figures 1 and 2 show that the migration velocity and the amplitude decay time strongly depend on kL_A, i.e. the ratio of wave length L ($2\pi/k$) and the suspension adjustment lenght L_A. Moreover, the ratio suspended-load transport /bed-load transport q_s/q_b has a considerable influence on the morphodynamic behaviour.

Remark:
It should be realized that $\tilde{c}_{bed}$ and $\tilde{T}_{bed}$ are made non-dimensional using q_b, which also appears in the parameter q_s/q_b. This parameter should therefore be considered as a suspended-load transport parameter only (q_b is constant), when the plots are used to study the behaviour of the dimensional values c_{bed} and T_{bed}.

The amplitude decay time strongly decreases for decreasing wave lenght due to increasing bed-slope effects. For long bed waves increasing suspension leads to shorter decay times, while for short bed waves suspension hardly affects the decay time (dominant bed-load).
Also the migration velocity is minimum for short waves ($L \ll L_A$ or $kL_A \gg 1$), when the bed-load transport controls the morphodynamic behaviour, and maximum for long waves ($L \gg L_A$ or $kL_A \ll 1$) when bed-load as well as suspended-load contribute to it.
In general, for very short waves ($L \ll L_A$) suspended does not affect the morphodynamics, although it may dominate the total transport rate.

Using (38a), (39a), (6a), (34a) and (36a) the expressions (48a,b) can be written also as function of a number of non-dimensional flow/sediment parameters and transport model coefficients as follows:

$$\tilde{c}_{bed} = 1 + \frac{\frac{4}{3}\frac{\varepsilon_s}{\varepsilon_b}\tan\varphi\frac{\alpha_s^4}{\alpha_b^3}\frac{C}{\sqrt{g}}\left|\frac{u_{*_0}}{W_s}\right|}{\tilde{L}^2\frac{C^2}{g}\left(\frac{u_{*_0}}{W_s}\right)^2 k^2 h_0^2 + 1} \tag{49}$$

$$\tilde{T}_{bed} = \left\{(kh_0)^2\left[\frac{\frac{4}{3}\tilde{L}\frac{\varepsilon_s}{\varepsilon_b}\tan\varphi\frac{\alpha_s^4}{\alpha_b^3}\frac{C^2}{g}\left(\frac{u_{*_0}}{W_s}\right)^2}{1+\tilde{L}^2\frac{C^2}{g}\left(\frac{u_{*_0}}{W_s}\right)^2 k^2 h_0^2} + \frac{1}{3\tan\varphi}\right]\right\}^{-1} \tag{50}$$

in which :

u_{*_0} = friction velocity in the basic state = $\frac{\sqrt{g}}{C}.u_0$ (only current)

W_s = settling velocity of sediment

C = Chezy coefficient

For a constant bed roughness (C) and selected values for the transport model coefficients only two parameters remain controlling the morphodynamic behaviour, i.e.:

- $kh_0 (= 2\pi h_0 / L)$: non-dimensional bed wave length

- u_* / W_s : non-dimensional settling velocity
  The ratio of bed shear velocity (due to current) and settling velocity of the sediment (suspension parameter). For large $u_{*_0} / W_s >> 1$ fully developed suspension can be expected, for values <<1 bed-load transport will be only present.

Using the standard efficiency factors of Bailard $\varepsilon_b = 0.1$, $\varepsilon_s = 0.02$ and selecting $\varphi =$ angle of repose=32^0, and the velocity and concentration profile coefficients $\alpha_b = \alpha_s = \widetilde{L} = 0.5$ it follows that:

(51) $$\widetilde{c}_{bed} = 1 + \frac{0.0833 \frac{C}{\sqrt{g}} \frac{|u_{*_0}|}{W_s}}{0.25 \frac{C^2}{g} (\frac{u_{*_0}}{W_s})^2 k^2 h_0^2 + 1}$$

(52) $$\widetilde{T}_{bed} = \left\{ (kh_0)^2 \left[\frac{0.042 \frac{C^2}{g} \left(\frac{u_{*_0}}{W_s} \right)^2}{1 + 0.25 \frac{C^2}{g} \left(\frac{u_{*_0}}{W_s} \right)^2 k^2 h_0^2} + 0.533 \right] \right\}^{-1}$$

In Figure 3 the non-dimensional migration velocity (51) is shown as a function of L/h_0 (bed-wave length / depth ratio = $2\pi/kh_0$) and of the suspension parameter u_*/W_s. The Chezy coefficient C = 50 $m^{1/2}/s$.

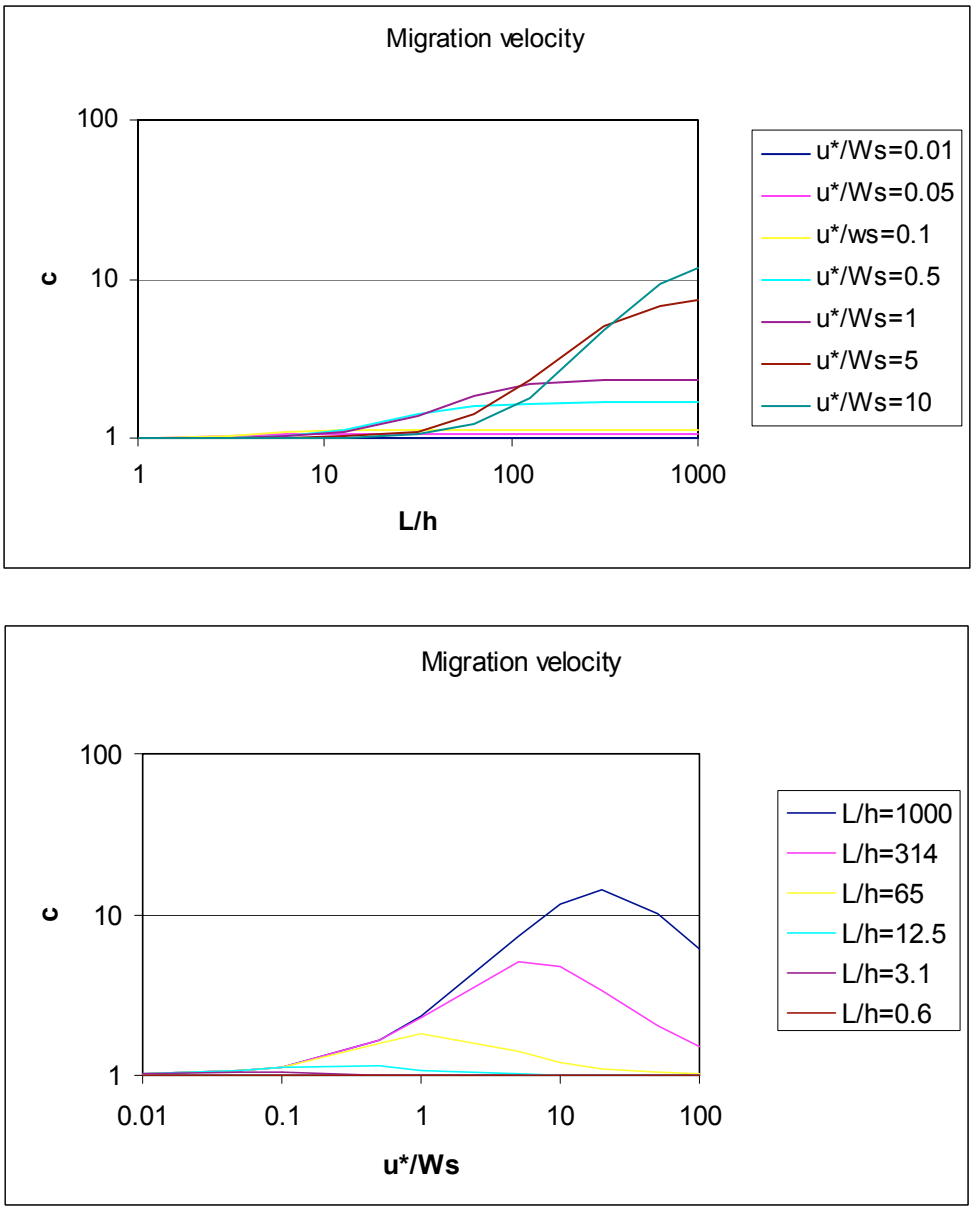

Figure 3 Non-dimensional migration velocity $\tilde{c}_{bed}$ as a function of the suspension parameter u_*/W_s and the bed wave length/depth ratio L/h. (C=50 $m^{1/2}/s$)

It is shown again that large wave length have a larger migration velocity than short bed waves, due to an increasing contribution of suspension (especially for large u_*/W_s). The relation between c and u_*/W_s shows a maximum, due to the fact that – although the total transport rate increases with increasing u_*/W_s (more suspension), the contribution of suspension to migration decreases for large u_*/W_s due to spatial phase-lag effects (especially for short bed waves).

Figure 4 shows the non-dimensional amplitude decay time (52) as a function of L/h_0 .

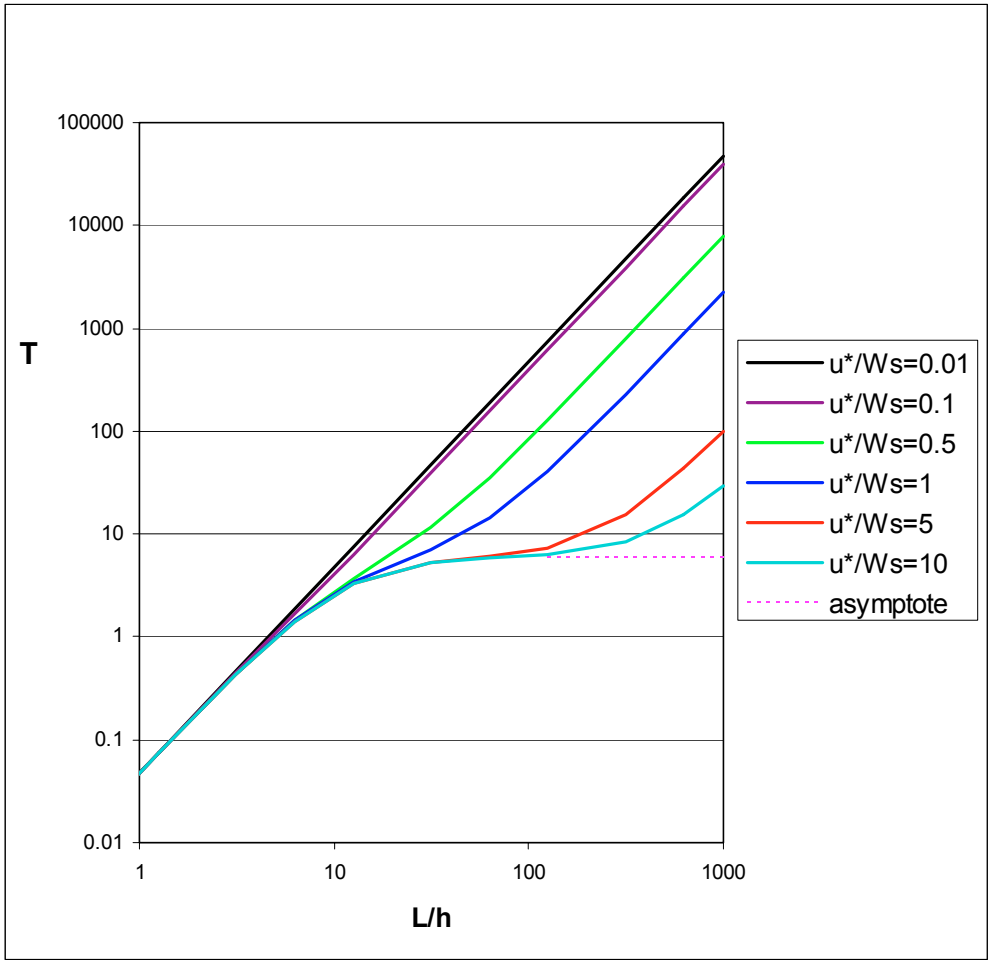

Figure 4 Non-dimensional amplitude-decay time $\widetilde{T}_{bed}$ vs. wave-length /depth ratio L/h for different values of the suspension parameter u_*/W_s (C=50 $m^{1/2}/s$)

It is shown that suspension (and the suspension parameter) does not affect the morphology for short bed waves (L/h < 10). In this regime bed-load and bed-slope effects control migration and amplitude decay. Suspension is present and may dominate the transport rate, but is not contributing to morphological changes since it cannot respond quick enough to the short bed-level variations (through deposition to and pick-up from the bed). In this regime suspension is only transported along, behaving as wash-load and fully controlled by the upstream influx.

The amplitude decay time increases strongly for increasing wave length (L/h ratio), primarily due to the decreasing influence of bed-slope. An increasing suspended-load/bed-load ratio (or suspension parameter u_*/W_s) speeds up amplitude decay strongly,

especially for long bed waves. For very large values u_*/W_s and for large wave lengths $10<L/h<1000$ the following horizontal asymptote is found :

(52a)

$$\widetilde{T}_{bed} = \left\{ \frac{4\varepsilon_s \tan\varphi \dfrac{\alpha_s^4}{\alpha_b^3}}{3\varepsilon_b \widetilde{L}} \right\}^{-1} \quad (=6.0)$$

Remark :
It should be realized that the scaling parameters of $\widetilde{c}_{bed}$ and $\widetilde{T}_{bed}$, i.e. $c_b^c (\approx u_0^3/h)$ and h, are not fully independent of u_*/W_s and L/h. Only for constant u_* and h, the shown behaviour of $\widetilde{c}_{bed}$ and $\widetilde{T}_{bed}$ is representative for the behaviour of the dimensional c_{bed} and T_{bed}. For this purpose the parameter u_*/W_s should be considered as a 'grain-size or settling velocity parameter ' and L/h as a 'bed wave-length' parameter.

Migration versus damping

Whether migration or damping dominates the morphological process can be analyzed with the following migration-damping ratio MD:

(52b)

$$MD = \frac{c_{bed}}{\frac{1}{2}L}.T_{bed} = \frac{\widetilde{c}_{bed}\widetilde{T}_{bed}}{\frac{1}{2}L/h}$$

The parameter relates the the amplitude decay time T_{bed} (=time to reduce the amplitude with a factor e) to the time needed for migration of ½ a wavelength $c_{bed}/(\frac{1}{2}L)$. For $MD >> 1$ migration dominates, while for $MD << 1$ damping dominates.

Figure 5 shows the behaviour of the parameter MD. It is shown that for $L/h \approx 1$ (small wave lengths) damping dominates. Migration dominates for $L/h > 100$ (large wave lengths) in combination with dominant bed-load conditions ($u_*/W_s<<1$). For intermediate wave lengths $10<L/h<100$ migration and damping will both be present.

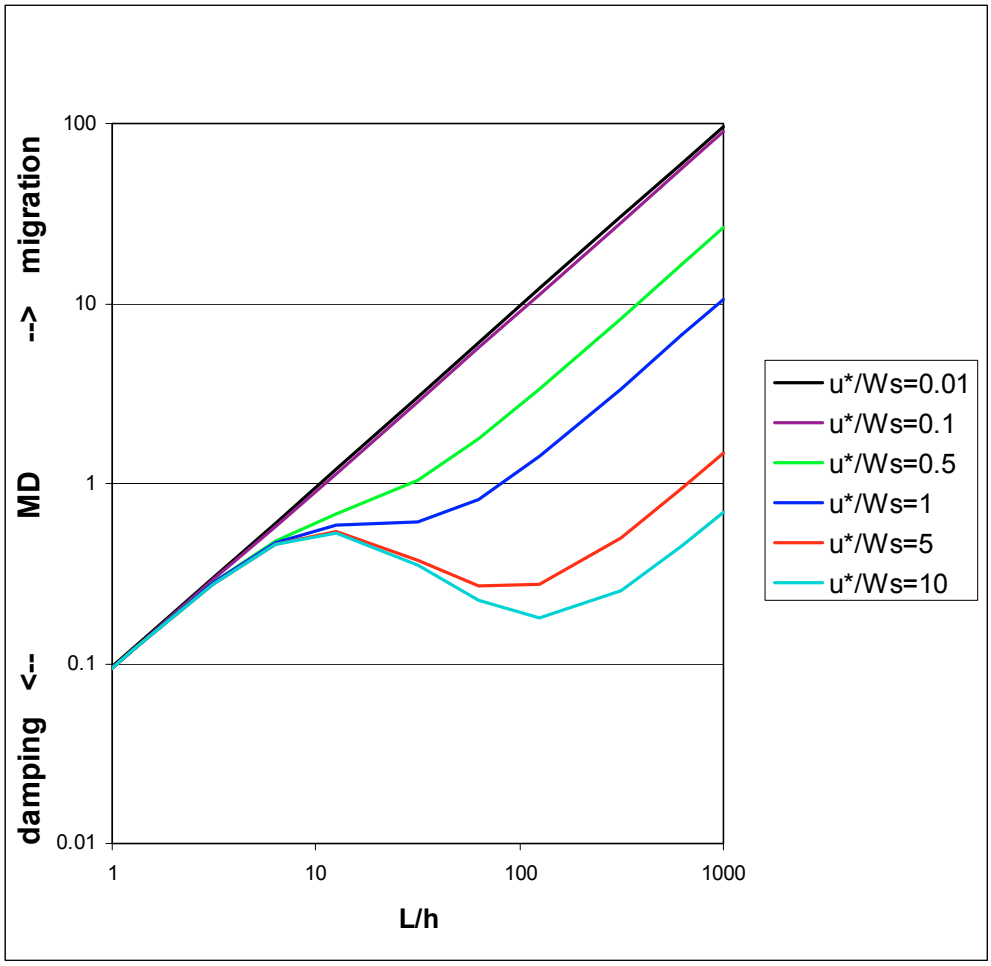

Figure 5 Damping or migration dominates depending on the parameters L/h and u_*/W_s (C=50 $m^{1/2}/s$)

5 Steady current and waves

For the situation of current and waves, only the derivation of the expressions for 'current dominated' conditions is given here. For wave –dominated conditions the derivation and the resulting expressions are given in Appendix D .

Substituting of (38a,b) and (39a,b) into the full expression (45) gives:

(53)

$$\widetilde{c}_{bed} = 1 + \frac{\frac{4}{3}\frac{\varepsilon_s}{\varepsilon_b}\tan\varphi\frac{\alpha_s^4}{\alpha_b^3}\frac{C}{\sqrt{g}}\frac{|u_{*0}|}{W_s}}{\widetilde{L}^2\frac{C^2}{g}\left(\frac{u_{*0}}{W_s}\right)^2 k^2 h_0{}^2 + 1} + \frac{1}{6}\frac{1}{\alpha_b^2}\left(\frac{\hat{U}_0}{u_0}\right)^2(1+2f) + \frac{\frac{1}{2}\frac{\varepsilon_s}{\varepsilon_b}\tan\varphi\frac{\alpha_s^2}{\alpha_b^3}\frac{C}{\sqrt{g}}\frac{|u_{*0}|}{W_s}\left(\frac{\hat{U}_0}{u_0}\right)^2(1+f)}{\widetilde{L}^2\frac{C^2}{g}\left(\frac{u_{*0}}{W_s}\right)^2 k^2 h_0{}^2 + 1}$$

with f according to (38c).

Using linear wave theory for $\hat{U}_0$ (3) this can be written as :

(54)
$$\widetilde{c}_{bed} = 1 + \frac{1}{6}\frac{1}{\alpha_b^2}\left(\frac{\pi H_0}{T u_0}\right)^2\frac{(1+2f)}{\sinh^2 k_w h_0} + \widetilde{c}_s^c\left[1 + \frac{3}{8}\frac{1}{\alpha_s^2}\left(\frac{\pi H_0}{T u_0}\right)^2\frac{(1+f)}{\sinh^2 k_w h_0}\right]$$

or rewriting $\pi H / T u_0$ using $k_{w_\infty} = \frac{4\pi^2}{gT^2}$ gives:

(55)

$$\widetilde{c}_{bed} = 1 + \underbrace{\frac{1}{24}\frac{1}{\alpha_b^2 Fr^2}k_{w_\infty}h_0\left(\frac{H_0}{h_0}\right)^2\frac{(1+2f)}{\sinh^2 k_w h_0}}_{\text{wave effect bed-load}} + \widetilde{c}_s^c\left[1 + \underbrace{\frac{3}{32}\frac{1}{\alpha_s^2 Fr^2}k_{w_\infty}h_0\left(\frac{H_0}{h_0}\right)^2\frac{(1+f)}{\sinh^2 k_w h_0}}_{\text{wave effect suspended-load}}\right]$$

with:

(55a)
$$\widetilde{c}_s^{\,c} = \frac{\frac{4}{3}\frac{\varepsilon_s}{\varepsilon_b}\tan\varphi\,\frac{\alpha_s^4}{\alpha_b^3}\frac{C}{\sqrt{g}}\frac{|u_{*0}|}{W_s}}{\widetilde{L}^2\frac{C^2}{g}\left(\frac{u_{*0}}{W_s}\right)^2 k^2 {h_0}^2 + 1}$$

(55b)
$$f = \frac{k_{w_\infty} h_0 . \sinh(2k_w h_0)}{(2k_w h_0 + \sinh(2k_w h_0)) . \tanh^2(k_w h_0)}$$

Without waves: $\widetilde{c}_{bed} = 1 + \widetilde{c}_s^{\,c}$ (see (49))

Using (38), (39), (40) and (6a) in combination with (46) gives for the amplitude decay time in a similar way :

(56)
$$\widetilde{T}_{bed} = \left\{ \frac{1}{\widetilde{T}_s^{\,c}} \left[1 + \frac{3}{8}\frac{1}{\alpha_s^2}\left(\frac{\pi H_0}{T u_0}\right)^2 \frac{(1+f)}{\sinh^2 k_w h_0} \right] + \frac{1}{\widetilde{T}_b^{\,c}} \left[1 + \frac{3}{4}\frac{1}{\alpha_b^2}\left(\frac{\pi H_0}{T u_0}\right)^2 \frac{1}{\sinh^2 k_w h_0} \right] \right\}^{-1}$$

or rewriting $\pi H / T u_0$ using $k_{w_\infty} = \frac{4\pi^2}{g T^2}$ gives:

(57)
$$\widetilde{T}_{bed} = \left\{ \frac{1}{\widetilde{T}_s^{\,c}} \left[1 + \frac{3}{32}\frac{1}{\alpha_s^2 Fr^2} k_{w_\infty} h_0 \left(\frac{H_0}{h_0}\right)^2 \frac{(1+f)}{\sinh^2 k_w h_0} \right] + \frac{1}{\widetilde{T}_b^{\,c}} \left[1 + \frac{3}{16}\frac{1}{\alpha_b^2 Fr^2} k_{w_\infty} h_0 \left(\frac{H_0}{h_0}\right)^2 \frac{1}{\sinh^2 k_w h_0} \right] \right\}^{-1}$$

wave effect suspended-load

wave effect bed-load /bed slope

with:

(57a)
$$\widetilde{T}_s^{\,c} = \left\{ (kh_0)^2 \frac{\frac{4}{3}\widetilde{L}\frac{\varepsilon_s}{\varepsilon_b}\tan\varphi\frac{\alpha_s^4}{\alpha_b^3}\frac{C^2}{g}\left(\frac{u_{*_0}}{W_s}\right)^2}{1+\widetilde{L}^2\frac{C^2}{g}\left(\frac{u_{*_0}}{W_s}\right)^2 k^2 h_0^2} \right\}^{-1}$$

(57b)
$$\widetilde{T}_b^{\,c} = \left\{ \frac{(kh_0)^2}{3\tan\varphi} \right\}^{-1}$$

Without waves: $\widetilde{T}_{bed} = \left\{ \frac{1}{\widetilde{T}_s^{\,c}} + \frac{1}{\widetilde{T}_b^{\,c}} \right\}^{-1}$ (see (48b))

In (55) and (57) two new non-dimensional parameters account for the effect of waves, i.e.

- $\frac{H_0}{h_0}$ = non-dimensional 'wave height' parameter
- $k_{w_\infty} h_0 = 4\pi^2 \frac{h_0}{gT^2}$ = non-dimensional 'wave period' parameter

Remark:
The water depth h_0 in these expressions as well as u_0 and h_0 in the Froude number Fr are also used for the scaling of c_{bed} and T_{bed}. Only for constant values of u_0 and h_0 the expressions (55) and (57) are representative for the non-scaled migration velocity and amplitude decay behaviour.

Similar expressions as (55) and (57) are derived for wave-dominant conditions (see Appendix D).

Using again the standard efficiency factors of Bailard $\varepsilon_b = 0.1$, $\varepsilon_s = 0.02$ and selecting φ = angle of repose=32^0, and the velocity and concentration profile coefficients $\alpha_b = \alpha_s = \widetilde{L} = 0.5$, (55) and (57) can be written as:

(58)
$$\widetilde{c}_{bed} = 1 + \frac{1}{6}\frac{k_{w_\infty} h_0}{Fr^2}\left(\frac{H_0}{h_0}\right)^2 \frac{(1+2f)}{\sinh^2 k_w h_0} + \widetilde{c}_s^{\,c}\left[1 + \frac{3}{8}\frac{k_{w_\infty} h_0}{Fr^2}\left(\frac{H_0}{h_0}\right)^2 \frac{(1+f)}{\sinh^2 k_w h_0}\right]$$

(58a)
$$\widetilde{c}_s^{\,c} = \frac{0.0833\dfrac{C}{\sqrt{g}}\dfrac{|u_{*0}|}{W_s}}{0.25\dfrac{C^2}{g}\left(\dfrac{u_{*0}}{W_s}\right)^2 k^2 {h_0}^2 + 1}$$

(58b)
$$f = \frac{k_{w_\infty} h_0 .\sinh(2k_{w_0} h_0)}{(2k_{w_0} h_0 + \sinh(2k_{w_0} h_0)).\tanh^2(k_{w_0} h_0)}$$

(59)
$$\widetilde{T}_{bed} = \left\{ \frac{1}{\widetilde{T}_s^{\,c}} \left[1 + \frac{3}{8} \frac{k_{w_\infty} h_0}{Fr^2} \left(\frac{H_0}{h_0} \right)^2 \frac{(1+f)}{\sinh^2 k_w h_0} \right] + \frac{1}{\widetilde{T}_b^{\,c}} \left[1 + \frac{3}{4} \frac{k_{w_\infty} h_0}{Fr^2} \left(\frac{H_0}{h_0} \right)^2 \frac{1}{\sinh^2 k_w h_0} \right] \right\}^{-1}$$

(59a)
$$\widetilde{T}_s^{\,c} = \left\{ (kh_0)^2 \frac{0.042\dfrac{C^2}{g}\left(\dfrac{u_{*_0}}{W_s}\right)^2}{1 + 0.25\dfrac{C^2}{g}\left(\dfrac{u_{*_0}}{W_s}\right)^2 k^2 h_0^2} \right\}^{-1}$$

(59b)
$$\widetilde{T}_b^{\,c} = \left\{ \frac{(kh_0)^2}{3\tan\varphi} \right\}^{-1}$$

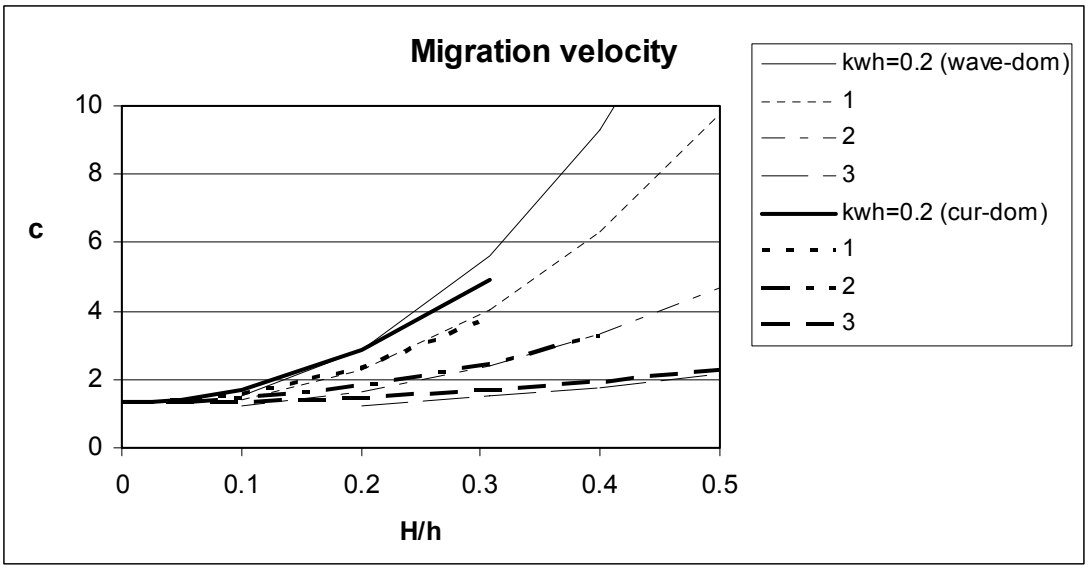

Figure 6 Influence of waves on the non-dimensional migration velocity through the wave height parameter H/h and the wave period parameter $k_{w_\infty} h$ (Fr=0.11, u_*/W_s=1.61, L/h=35, C=50 $m^{1/2}/s$, $\varphi=32^0$)

Figure 6 shows the influence of the wave parameters H/h and $k_{w_\infty} h_0$ for constant Froude number (Fr=0.1). For a selected water depth, H/h can be interpreted as wave height parameter and $k_{w_\infty} h_0$ ($=4\pi^2 \frac{h_0}{gT^2}$) as wave period parameter. Both the 'wave-dominant' as well as the 'current-dominant' expressions are shown. Their intersection point marks the transition of their validity range (for larger H/h : wave-dominant , for smaller H/h: current- dominant).

Especially large wave heights and large wave periods, being responsible for relatively large orbital velocities near the sea bed, can have a considerable effect on the migration velocity.
The amplitude decay may also reduce considerably through the presence of waves, as shown in Figure 7.

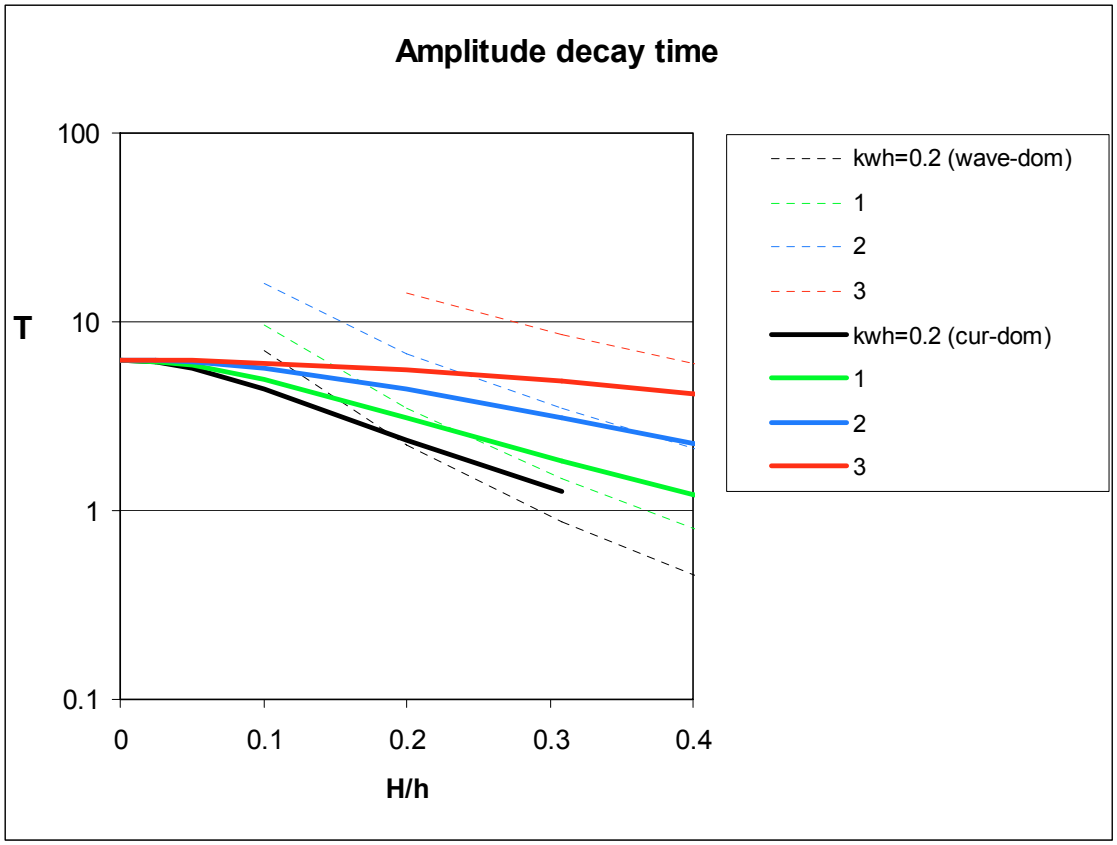

Figure 7 Influence of waves on the non-dimensional amplitude decay time through the relative wave height parameter H/h and the relative wave period parameter $k_{w_\infty} h$ (Fr=0.11, u_*/W_s=1.61, L/h=35, C=50 $m^{1/2}/s$, $\varphi=32^0$).

Migration versus damping

Although waves considerably accelerate the morphodynamic process, the character of the process is not much influenced. Since waves lead to a similar increase of the migration velocity as the decrease of the amplitude decay time, the migration/damping ratio MD is hardly affected by the waves. Figure 8 shows that only for relatively short bed waves, the MD parameter is reduced somewhat by the presence of waves.

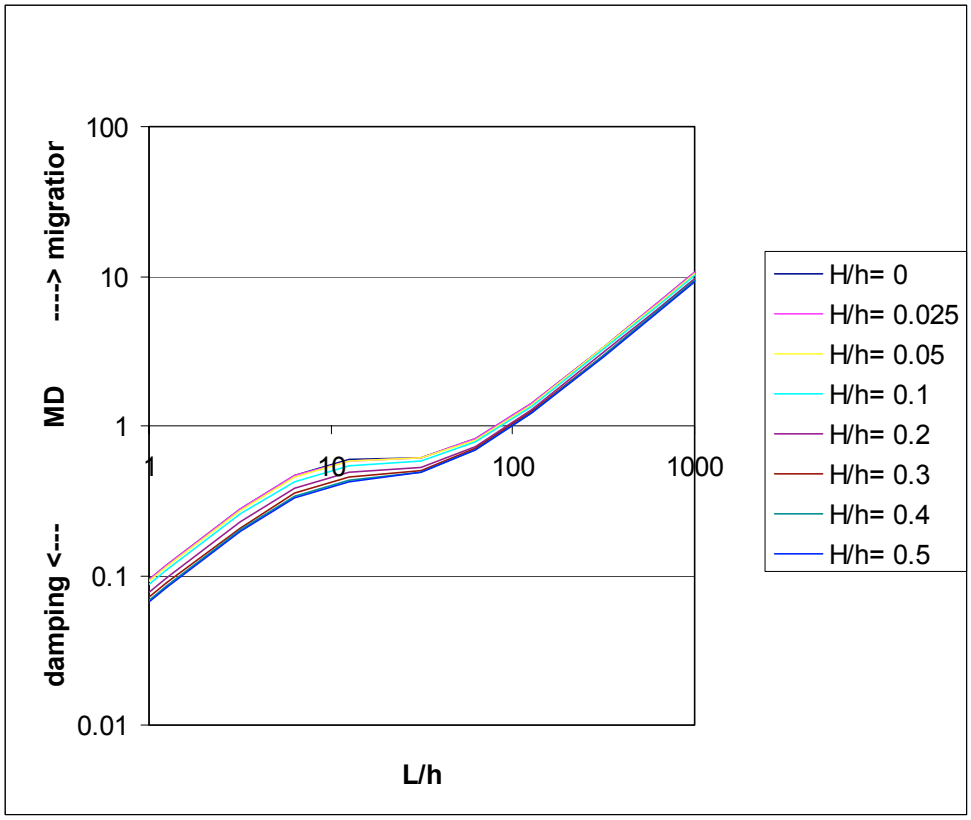

Figure 8 Migration-Damping parameter MD is hardly affected by the waves ($u_*/W_s = 1$, $k_{w_\infty} h_0 = 1$, C=50 $m^{1/2}/s$)

6 Validation of the analytical method with numerical computations of trenches

6.1 General

In order to verify whether the analytical method, based on harmonic analysis of sinusoidal bed waves, is also suitable for the description of trench morphodynamics the method is validated with a series of trench computations with the numerical model LOMOR, which solves the same basic equations numerically (Ribberink and Buijsrogge, 2003; see Appendix E).
The numerical values of migration velocity of the trench and amplitude-decay time of the trench (= trench infill time) are compared with the analytical values. The first comparison (section 6.3) is aimed at providing insight in possible differences due to the different shapes involved, i.e. sinusoidal bed waves (analytical method) on the one hand and a singular more trapezium shape of a trench on the other hand. A second comparison (section 6.4) is focusing on the influence of non-linear behaviour of trenches with a finite depth. The question is addressed is whether the results of the linear harmonic analysis can still be used in a sensible way.
To start with LOMOR is applied to a set of sinusoidal bed waves with a very small amplitude/water depth ratio in order to verify the analytical method in conditions in which the method should be (almost) exact (section 6.2).

6.2 Sinusoidal waves

LOMOR computations are carried out for a horizontally uniform wave-current situation over a sinusoidal bed, consisting of 5 wave lengths. On both sides of these 5 waves a horizontal bed is assumed. Three different wave lengths are considered, i.e. L=0.9 m, L=9 m and L=90 m. The following hydraulic/sediment conditions are selected on the basis of a laboratory experiment, which is used as benchmark case in the EU-project Sandpit (Benchmark II, see Appendix E) :

Depth-averaged velocity	u=0.18 m/s
Mean water depth	h=0.26 m
Wave height	H=0.08 m
Wave period	T=1.5 s
Settling velocity sediment	W_s=0.007 m/s

A very small amplitude A is assumed for the bed waves (A=1 mm), in order to create linear conditions (A/h<<1) , i.e. more or less constant conditions along the sine shape. In this way the linear analytical method should be more or less exact.

The following parameter settings are used for the (analytical and numerical) modelling:
The standard efficiency factors for the Bailard model $\varepsilon_b = 0.1$, $\varepsilon_s = 0.02$,
φ = angle of repose=32^0, and the velocity and concentration profile coefficients
$\alpha_b = \alpha_s = \widetilde{L} = 0.5$.

ρ = 1000 kg/m3 density of water
ρ_s = 2650.0 kg/m3 density of sediment
$\upsilon = 10^{-6}$ m2/s kinematic viscosity
k_w= 0.035 m roughness height
A calibration constant α_{cal} is used for the sediment transport (for bed-load and for suspended-load), α_{cal}=0.45 (see Appendix E). Finally, the model of Swart (1974) is used for the calculation of the friction coefficient.

The main computational results are shown in the Figures 6.1…6.3.
Figure 6.1 shows the LOMOR results of 2 sine waves (of the series of 5) for the example case with longest wave length (L=90 m) for a period of 40 hours. The migration and damping character of the sine waves is clearly represented by the model.

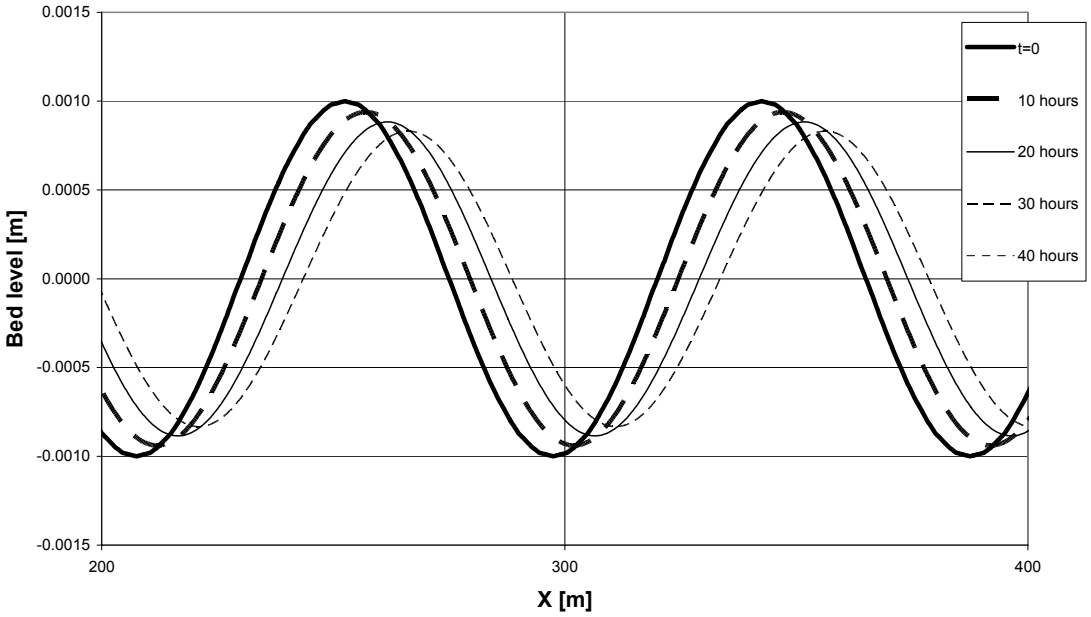

Figure 6.1 Sinusoidal bed wave morphodynamics (L=90 m) according to the numerical model LOMOR

.

Figure 6.2 shows the behaviour of the migration velocity as a function of the wave length, according to LOMOR and the 2 analytical approximations (wave-dominated and current dominated).

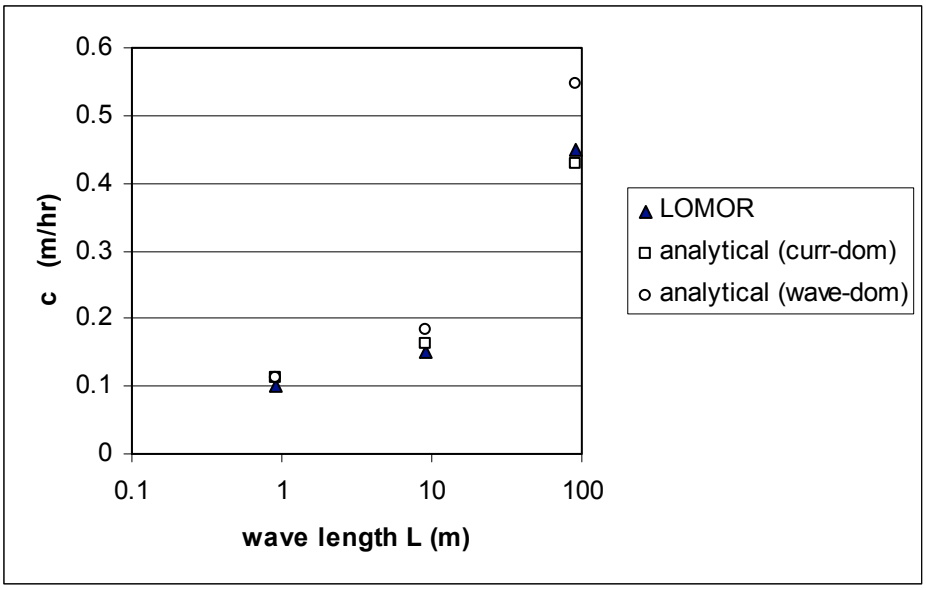

Figure 6.2 Migration velocity of sine waves : numerical (LOMOR) and analytical values

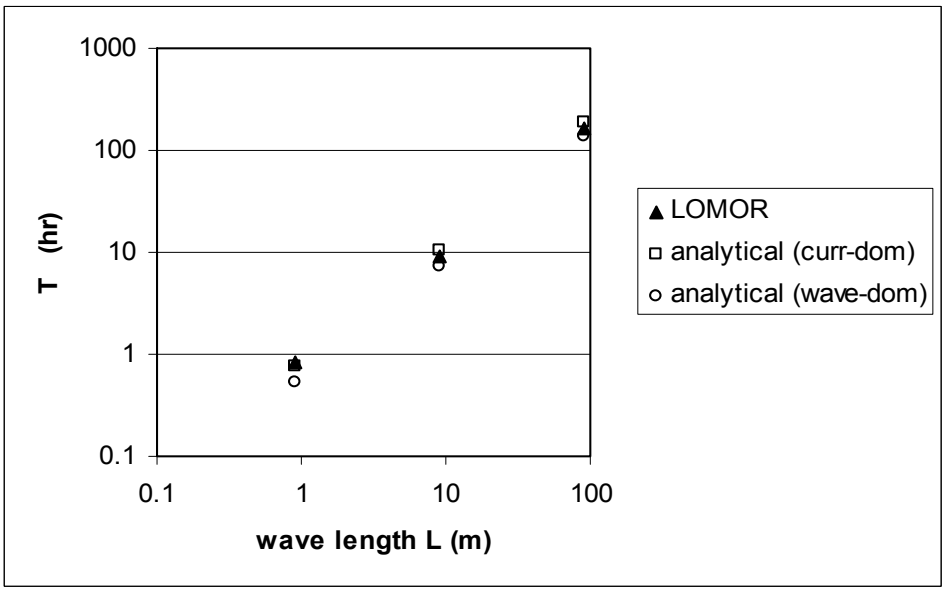

Figure 6.3 Amplitude decay time of sine waves : numerical (LOMOR) and analytical values

In general both methods show a very good agreement. The three selected wave lengths cover a wide L/h –range (3.5 – 350), in which the influence of the wave length on migration and decay is considerable.

6.3 Trapezium-shaped trenches

It is studied whether the migration and decay of (a series of) sine waves is of some use to predict migration and decay of a singular trapezium-shaped trench. Again the Benchmark II hydraulic/sediment conditions are used, but now three trapezium shaped trenches are assumed with trench lengths L_{trench} =0.45, 4.5 and 45 meters. For comparison purposes the trench lengths are assumed to be half of the wave lengths of the previous sinusoidal waves (L_{trench}=0.5L). Moreover, the trench depth D is set equal to the amplitude A of the sine waves (D=A=1mm). The shape of the three trenches is constant, i.e. the length of the sloping edges is also scaled with the trench length.

Figure 6.4 shows LOMOR results. Since spatial-scale and time-scale are directly coupled in morphodynamics also different simulation periods are depicted (also factor 10 difference, with the shortest period for the shortest trench). It can be observed that migration of the trench (advection) becomes increasingly important for increasing trench length, which is in general agreement with the analytical results.

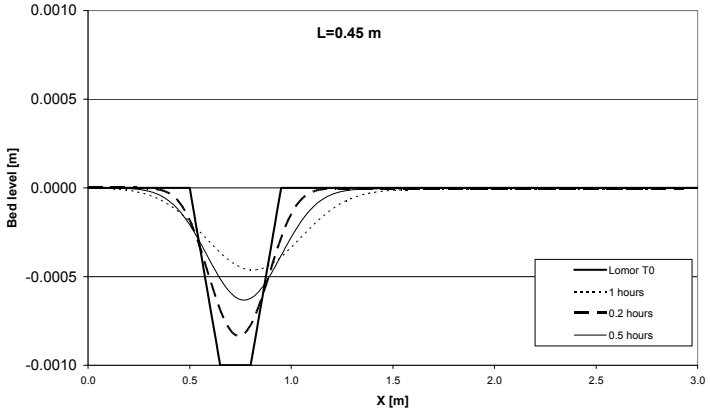

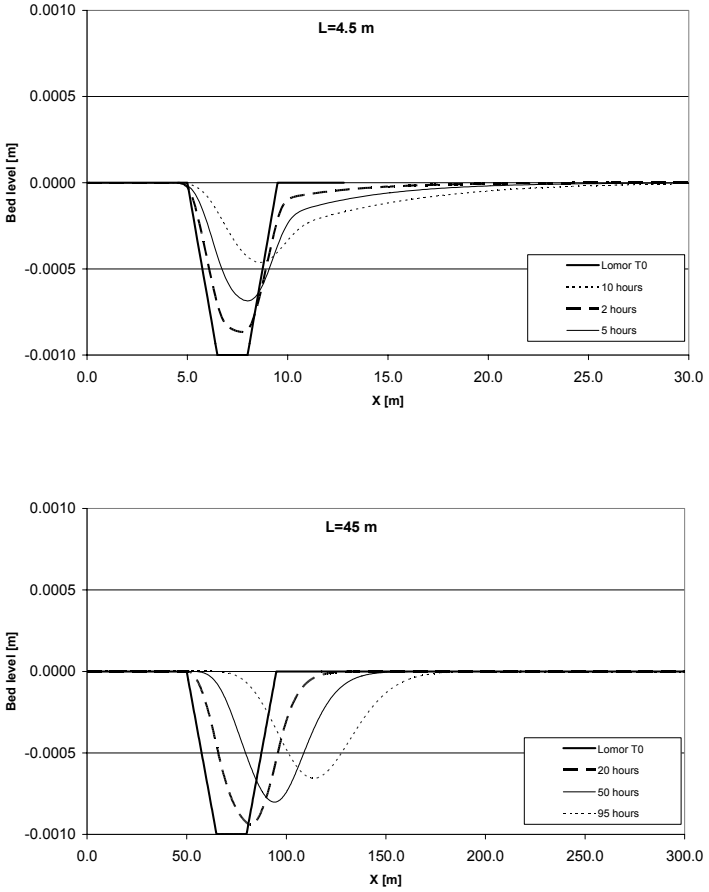

Figure 6.4 Morphodynamics of trapezium-shaped trenches with different length according to the numerical LOMOR model

For the trench with medium length (L=4.5 m) the morphological development shows an asymmetry, i.e. a difference is present between the development of the upstream and downstream slopes. This can be explained by the fact that for this trench, the trench length is approximately of the same magnitude as the adjustment length for suspension (L_A=3.3 m). Upstream of the trench suspension is in equilibrium, however downstream of the trench the suspended sediment needs distance (of order L_A) to re-adjust itself the basic state equilibrium conditions. For the medium lenght trench L/h ≈20 and $u_*/W_s \approx 1$. Both slopes are influenced by diffusion in a similar way, which can therefore not lead to any asymmetry. However, diffusion explains the fact that the steepening of the upstream slope is not visible in the results.
For the shorter trench case suspension adjustment is of only minor importance because $L_A << L_{trench}$. For the longer trench $L_A >> L_{trench}$ and again suspension adjustment is of minor importance.

A numerical migration velocity is calculated on the basis of the LOMOR results using the migration of the deepest point of the trench.

A numerical amplitude decay time is calculated on the basis of the decay of the trench depth in time (e-folding period). This is indicated in the following as '*trench infill time*'.

In Figure 6.5 the numerical migration velocity is plotted together with the analytical result c_{bed} (current-dominated approximation). The latter varies between a minimum value for infinitely short wave lengths $L<<L_A$) and a maximum value (for infinitely large wave lengths $L>>L_A$), which are also depicted in the figure.

- $L<<L_A$: suspended-load is present but only bed-load dominates the migration ($c_{bed}=c_b$, see Equations 41a, 38 and 39)
- $L>>L_A$: supended-load fully contributes to migration (lag-effects are negligible) ($c_{bed}=c_b+c_s$)

The analytical model agrees very well with the numerical result. Also LOMOR clearly shows the increasing migration velocity for increasing trench length. The (numerical) trench infill time is also well described by the analytical decay time T_{bed}.

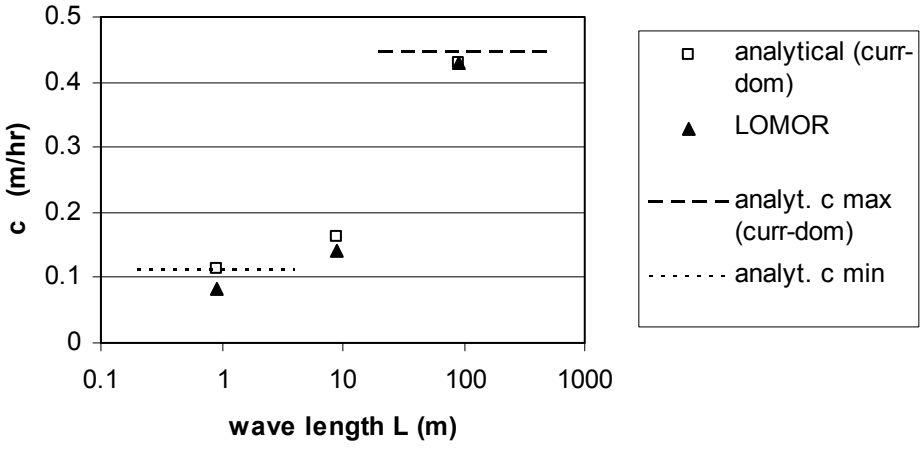

Figure 6.5 Migration velocity of trapezium-shaped trenches: numerical (LOMOR) and analytical values

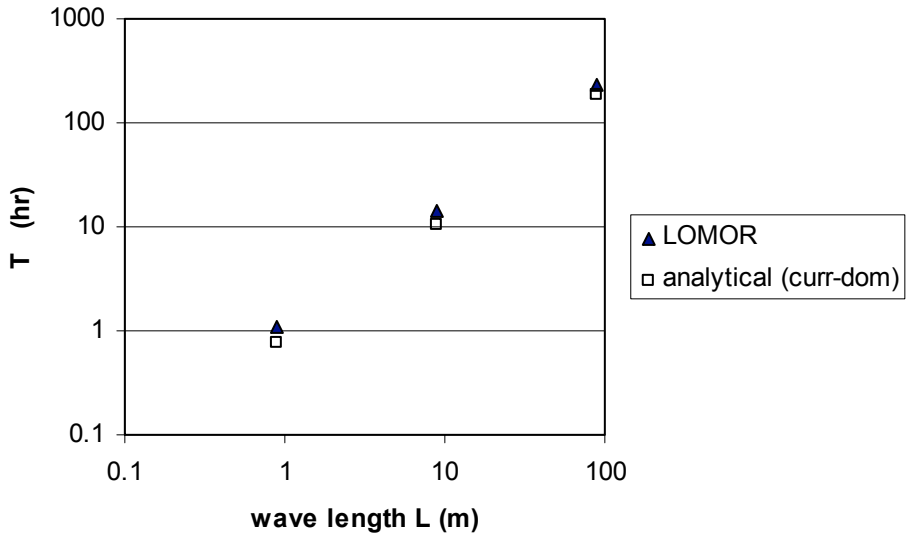

Figure 6.6 Infill time of trapezium-shaped trenches: numerical (LOMOR) and analytical values

6.4 Deeper trenches, non-linear cases

Is the linear harmonic analysis also useful for deeper trenches, when non-linear effects enter the problem ?
To answer this question the three BM2 trapezium-shaped trenches (with lengths 0.45, 4.5 and 45 m) are computed again with LOMOR, but now using three trench depths D (0.1 cm , 1.25 cm and 12.5 cm). With an (undisturbed) water depth h = 26 cm, this leads to three trench depth/ water depth ratio's D/h =0.004, 0.05 and 0.5. In total now 9 cases with different trench length/depth combinations are computed with LOMOR.

The general influence of increasing trench depth is an increasing deformation of the trench shape, with a steep upstream slope and a gradually more gentle downstream slope. Moreover, the trench migration reduces as well as its infill time. This is all depicted in Figure 6.7 for the 45 m long trench with the smallest (D/h=0.004) and largest trench depth (D/h=0.5). The vertical scale is normalized with the initial trench depth, so shape differences can be observed more easily.
Comparing the numerical trench migration velocities with the analytical values c_{bed} (Figure 6.8) shows that the numerical values generally agree reasonably well with analytical solutions for the two smallest trench depths. For the largest trench depth (d/h=0.5) the numerical migration velocity becomes considerably smaller.

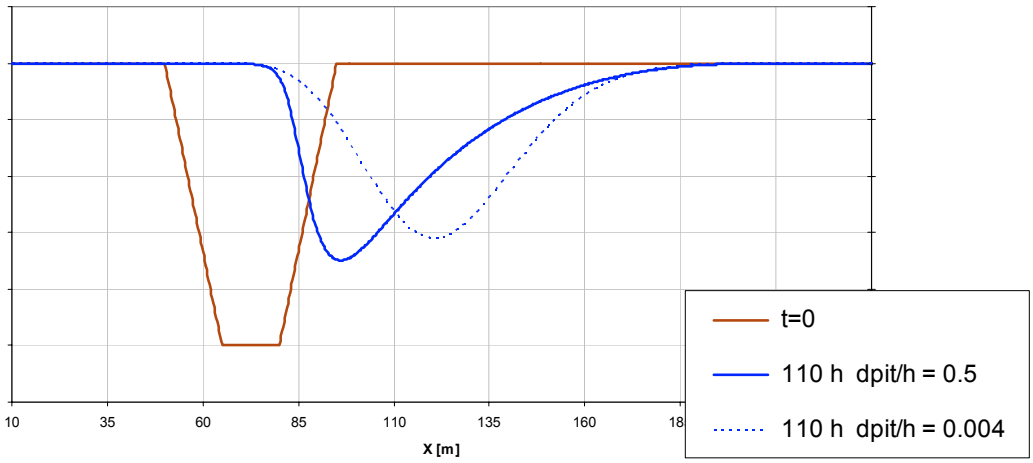

Figure 6.7 A shallow and a deep trench; the deep trench shows deformation and a reduced migration velocity and infill time.

The latter can be explained by the strongly reduced sediment transport rate in the deeper parts of the trench in comparison with the 'undisturbed' sea-bed situation (basic state). This is due to the fact that wave- and current induced velocities are strongly reduced in these parts (non-linear effect). Consequently, the morphodynamic process (i.e. migration and infill) is also slowed down strongly in these deeper trench parts (see Figure 6.7).

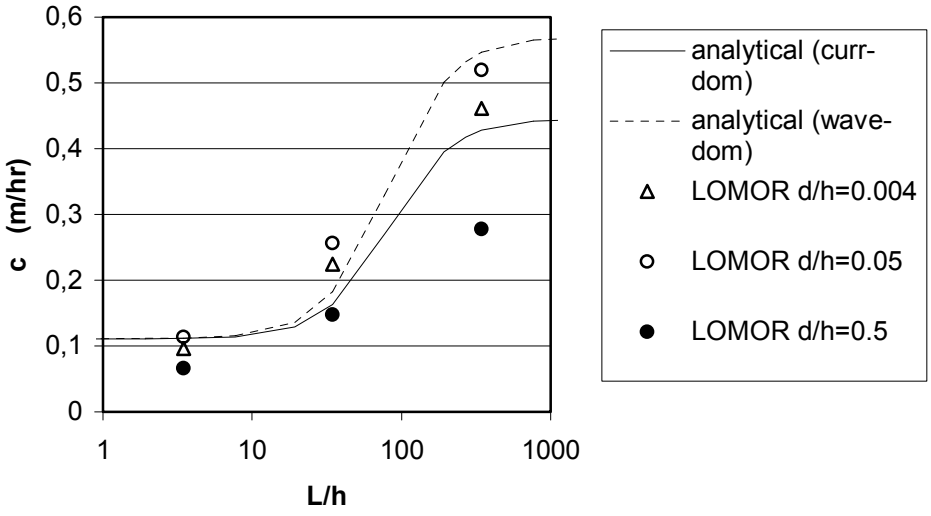

Figuur 6.8 Trench migration velocity: analytical model (dashed and full line) and LOMOR results for a small, medium and large trench depth (d/h ratio).

Similarly, the trench infill slows down especially for the deepest trench cases. Figure 6.9 shows the numerical infill time and the analytical infill time T_{bed} for the 9 cases.

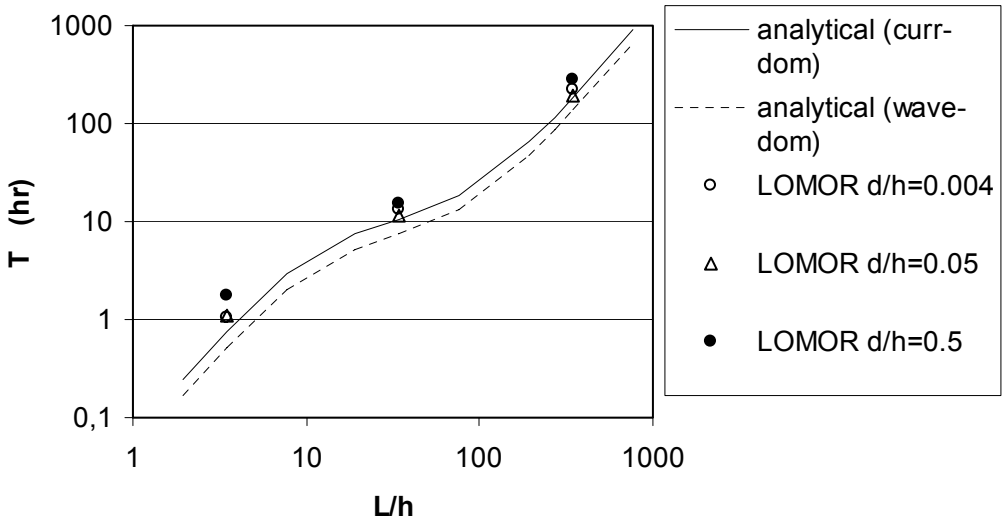

Figure 6.9 Trench infill time: analytical model (dashed and full line) and LOMOR results for a small, medium and large trench depth/water depth d/h ratio.

6.5 Non-linear analytical approximation for deep (and shallow) trenches

In order to overcome the worse performance of the analytical model for deep trenches an approximative non-linear solution is proposed. The non-linear solution is constructed on the basis of the expressions for migration velocity c_{bed} and infill time T_{bed} for two basic state conditions, namely at the undisturbed sea bed level (= basic state of the original linear analytical model) and at the bottom of the trench. By taking the average value for the two states of migration velocity and of the growth rate (=1/T_{bed}) the following non-linear approximation is obtained:

(60)

$$\overline{c}_{bed} = (c_{bed_0} + c_{bed_1})/2$$

$$\overline{T}_{bed} = \left\{\left(T_{bed_0}^{-1} + T_{bed_1}^{-1}\right)/2\right\}^{-1}$$

With indices '0' and '1' referring to respectively 'undisturbed sea bed conditions' and 'conditions at the trench bottom'.

This method is applied to the BM2 cases as discussed in the previous sections for the 3 cases with the deepest trench (d/h=0.5). Conditions '0' at the 'undisturbed sea bed' are described in Section 6.2. The conditions '1' at the bottom of the (initial) trench can easily derived from the '0' conditions and are as follows:

Depth-averaged velocity	u=0.12 m/s
Mean water depth	h=0.39 m
Wave height (unchanged)	H=0.08 m
Wave period (unchanged)	T=1.5 s
Settling velocity sediment (unchanged)	W_s=0.007 m/s

The reduced velocities at the trench bottom lead to a factor 5 reduction of the bed-load related migration velocity $c_{b_c}\ (\cong u^3)$.

The LOMOR results are shown in the Figures 6.10 and 6.11 together with the original linear analytical model as well as with the new approximative non-linear solution. The analytical solution for current-dominated conditions is applied here. It is shown that the LOMOR results for the deepest trench cases (d/h=0.5) are much better described with the new approximative non-linear model.

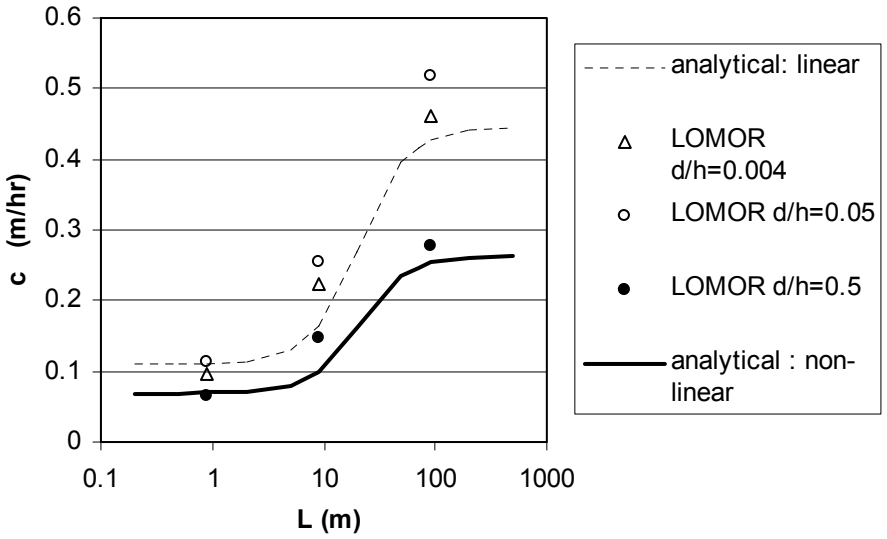

Figure 6.10 Approximative non-linear analytical solution (for d/h=0.5) gives a better description for the migration velocity of deep trenches.

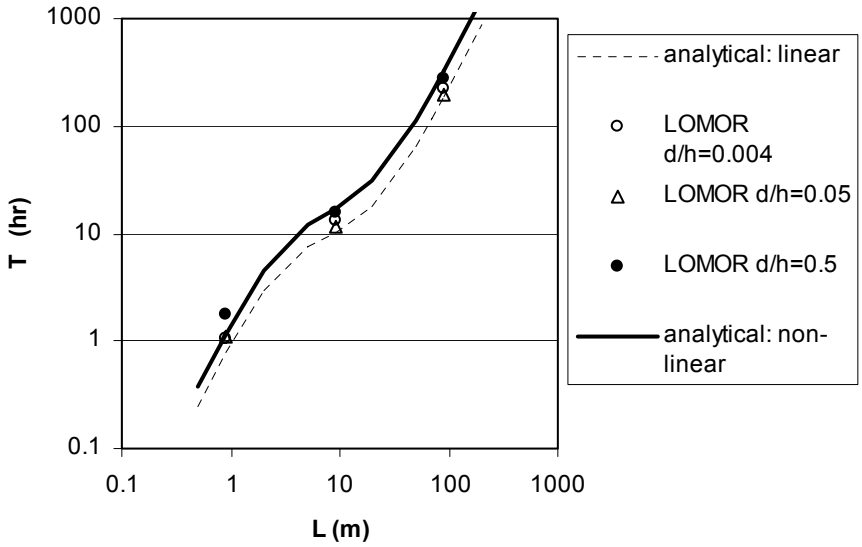

Figure 6.11 Approximative non-linear analytical solution (for d/h=0.5) gives a better description for the infill time of deep trenches.

7 Summary and conclusions

A 1D model describing the morphodynamic behaviour of dredged trenches under the influence of a current and surface waves (based on Ribberink, 1989) is developed further and analyzed. Considering short and shallow channels, the flow - normal to the axis of the channel - is assumed to be frictionless with Froude numbers $Fr<<1$. Short surface-wave characteristics are spatially constant and linear wave theory is assumed for the description of the near-bed wave orbital flow. Sediment transport is described with the transportformula of Bailard (1981) for the bed-load transport and a depth-averaged model for suspended sediment, including spatial lag effects, based on Galappatti and Vreugdenhil (1985) and Bailard (1981).

Linearizing the basic equations leads to one partial differential equation describing the bed-level dynamics. An harmonic analysis of the linearized model shows that sinusoidal bed-level waves (wave lengths L) generally migrate in the direction of the mean current and show decaying amplitudes in time (damping). Analytical expressions are derived for the migration velocity and the amplitude decay time. It is shown that the ratio of bed wave length and (undisturbed) water depth L/h and the Rouse suspension parameter u_*/W_s (u_*=bed-shear velocity, W_s=sediment settling velocity) are the main parameters controlling the morphodynamic process. New insights are obtained in the effects of suspended sediment and surface waves. Due to spatial lag effects, suspended sediment – although often dominating the sediment transport ($u_*/W_s>1$) – may only have a minor or no contribution to the morphodyamic process in case of relatively short bed waves ($L/h<20$). Amplitude- decay generally dominates the morphodynamics for these short bed waves ($1<L/h<10$-100), while migration is more dominant for long bed waves ($L/h>>10$-100). Bed-stirring effects of surface waves lead to a considerable acceleration of the morphodynamic processes. Controlling parameters are the relative height and lenght of the surface waves (H/h and k_wh , H=wave height and k_w='deep water' wave number). Two approximative solutions are derived for the situation of a current and waves, i.e. one for current-dominated and one for wave-dominated conditions.

An analytical parameter is derived (MD = migration-damping ratio), providing insight in the relative importance of migration or damping (= trench infill) for the morphodynamic process. It appears that this parameter is mainly affected by the trench length/ water depth ratio L/h and the suspension parameter u_*/W_s. Although surface waves considerably accelerate the morphodynamic process, they hardly affect the migration-damping ratio, indicating that the character of the morphodyamic process is rather insensitive for the presence of surface waves.

Whether the analytical expressions for migration velocity c_{bed} and amplitude decay time T_{bed} - in principle derived only for sinusoidal bed waves with infinitely small amplitudes - can also be used for describing the *migration velocity* and the *infill time* of singular trapezium-shaped trenches is then tested with numerical model results (LOMOR, Ribberink and Buijsrogge, 2003)

Numerical computations are carried out for a wide range of trench length L_{trench} – trench depth d_{trench} combinations (9 cases) and compared with the analytical model. In general the analytical formulas for c_{bed} and T_{bed} provide good approximations for the *migration velocity* and *infill time* of trapezium-shaped trenches with small trench depths (relative to the water depth). However, for large trench depths the migration velocity and the infill time are overestimated by the analytical model, due to non-linear effects.

More general approximative analytical formulas are therefore derived for trenches of variable (small and large) depth, using the mean analytical solutions of two basic state conditions, i.e. for 'undisturbed sea bed conditions' and 'conditions at the bottom of the trench'. Comparisons with the LOMOR computations show that this non-linear solution for trench migration velocity and trench infill time performs very well for deep trenches. This analytical model should therefore be prefered for trenches of variable depth.

The analytical expressions for *trench infill time* and *migration velocity* are derived for arbitrary wave – current combinations. In practical conditions of tidal flow and a wave climate the method can be applied for individual classes of wave –current combinations and weighed with their probabability of occurrence. Statistical mean values can then be determined.

References

Alphen, S.L.J. van, Hallie , F.P., Ribberink, J.S., Roelvink, J.A. and C.J. Loisse (1990), Offshore sand extraction and nearshore profile nourishment, Proc. 22nd Coast. Eng. Conf. ICCE, ASCE, Vol.2, p 1998-2009.

Bailard, J.A. (1981), An energetics total load model for a plane sloping beach, J. of Geoph. Res.86 (C11), 10938-10954.

Galappatti, R. and Vreugdenhil , C.B. (1985) , A depth-integrated model for suspended transport , J. of Hydr. Research, ASCE, Vol. 23, No. 4.

Jansen, P.Ph. (ed.) (1994), Principles of River Engineering – The non-tidal alluvial river, Delftse Uitgevers Maatschappij b.v., ISBN 90 6562 146 6, 1979

Ribberink, J.S. (1989), Zeezandwinning, WL | Delft Hydraulics, report H825 (in Dutch)

Ribberink, J.S. and R.H. Buijsrogge (2003), 1DH modeling of sand pit morphology in the marine environment: a numerical model, Technical Note EU project Sandpit, October 2003 (see Appendix E of the present report)

Roos, P.C. (2004), Seabed pattern dynamics and offshore sand extraction, Ph.D. Thesis University of Twente, ISBN 90-365-2067-3.

Swart, D.H. (1974), Offshore sediment transport and equilibrium beach profiles, Delft Hydr. Lab. Publ. No. 131, Delft Hydraulics, The Netherlands.

Appendix A Relation between spatial bed-level gradients and near-bed orbital velocity gradients according to linear wave theory

According to linear wave theory the near-bed horizontal orbital velocity is :

(A1) $$\hat{U} = \frac{\pi H}{T \sinh kh}$$

The dispersion relation relates the 'deep water' wave number k_0 to the local wave number k at depth h:

(A2) $$k_0 h = kh \tanh kh$$

with:

(A3) $$k_0 = \frac{4\pi^2}{gT^2}$$

Assuming a constant wave height H and period T , spatial gradients in $\hat{U}$ can be written as:

(A4)

$$\frac{\partial \hat{U}}{\partial x} = \frac{\partial \hat{U}}{\partial kh} . \frac{\partial kh}{\partial x} = \frac{\partial \hat{U}}{\partial kh} . \frac{\partial kh}{\partial k_0 h} . \frac{\partial k_0 h}{\partial x} = \frac{\partial \hat{U}}{\partial kh} . \frac{\partial kh}{\partial k_0 h} . k_0 \frac{\partial h}{\partial x} = f_3(kh) . k_0 \frac{\partial h}{\partial x}$$

Function f_3(kh) can be worked out as follows.

(A5) $$\frac{\partial \hat{U}}{\partial kh} = -\frac{\pi H}{T} \frac{\cosh kh}{\sinh^2 kh}$$

(A6)

$$\frac{\partial k_o h}{\partial kh} = \tanh kh + kh.\frac{\partial \tanh kh}{\partial kh} = \tanh kh + \frac{kh}{\cosh^2 kh} = \frac{\sinh kh \cosh kh + kh}{\cosh^2 kh}$$

With (A5) and (A6), (A3) becomes:

(A7) $$f_3(kh) = -\frac{\pi H}{T}\frac{\cosh kh}{\tanh^2 kh(kh + \sinh kh \cosh kh)}$$

Appendix B Wave –averaged bed-load transport and suspended-load transport power-law descriptions for combined waves and current

The near-bed intra-wave flow velocity u_b ,driving the sedimenttransport, is composed of a near-bed horizontal orbital flow velocity (oscillatory flow with amplitude $\hat{U}$) and, normal to this in x-direction, a near-bed steady mean flow velocity $\alpha_b u$ (u=depth-averaged velocity), with α_b a factor <1 which should be selected (standard α_b=0.5).

The *bed-load component in the direction of the steady current* (current-related component) according to the formula of Bailard (see (34)) can be written as:

(B1) $$q_b = m_b u_b^2 . u_{b_x} - m_b \frac{\partial z_b / \partial x}{\tan\varphi} \left| u_b^3 \right|$$

Because $u_{b_x} = \alpha_b u$ is constant during a wave period, the wave-averaged bed-load transport becomes:

(B2) $$q_b = m_b < u_b^2 > \alpha_b u - m_b \frac{\partial z_b / \partial x}{\tan\varphi} < \left| u_b^3 \right| >$$

The velocity moments $<u_b^2>$ and $<| u_b^3 |>$ can be expressed in the near-bed steady flow velocity $\alpha_b u$ and the near-bed wave orbital velocity amplitude $\hat{U}$ using simple analytical expressions.

$$u_b^2 = \alpha_b^2 u^2 + \tilde{U}^2$$

or wave-averaged:

$$< u_b^2 >= \alpha_b^2 u^2 + < \tilde{U}^2 >$$

Using linear wave theory with $\tilde{U} = \hat{U} \sin \omega t$:

(B3) $$< u_b^2 >= \alpha_b^2 u^2 + \frac{1}{2} \hat{U}^2$$

$| u_b^3 |$ can be written as:

$$|u_b^3| = (u_b^2)^{3/2} = (\alpha_b^2 u^2 + \tilde{U}^2)^{3/2}$$

For $\alpha_b^2 u^2 > \tilde{U}^2$ (current dominates over the wave) this can be approximated using a Taylor expansion as:

$$\left|u_b^3\right| = \alpha_b^3 \left|u^3\right| (1 + \frac{3}{2} \frac{\tilde{U}^2}{\alpha_b^2 u^2})$$

Wave-averaged using again linear wave theory this becomes:

(B4) $$< \left|u_b^3\right| >= \alpha_b^3 \left|u^3\right| + \frac{3}{4} \hat{U}^2 \alpha_b |u|$$

For $\tilde{U}^2 > \alpha_b^2 u^2$ (wave dominates over the current) :

$$\left|u_b^3\right| = (\tilde{U}^2)^{3/2} (1 + \frac{3}{2} \frac{\alpha_b^2 u^2}{\tilde{U}^2}) = (\tilde{U}^2)^{3/2} + \frac{3}{2} \alpha_b^2 u^2 (\tilde{U}^2)^{1/2} = \left|\tilde{U}^3\right| + \frac{3}{2} \alpha_b^2 u^2 \left|\tilde{U}\right|$$

Using linear wave theory $\tilde{U} = \hat{U} \sin \omega t$ and averaging over the wave period by integration (θ=ωt) :

$$\frac{1}{2\pi} \int_0^{2\pi} .. d\theta$$

and using the rule $\sin^3 \theta = \frac{3}{4} \sin \theta - \frac{1}{4} \sin 3\theta$ leads to:

(B5) $$< \left|u_b^3\right| >= \frac{4}{3\pi} \hat{U}^3 + \frac{3}{\pi} \alpha_b^2 u^2 \hat{U}$$

Using (B4) and (B5) the expression for the wave-averaged bed-load transport becomes:

(B6) $$q_b = m_b\left[\ \alpha_b^3 u^3 + \frac{1}{2}\alpha_b u\hat{U}^2\ \right] - m_b \frac{\partial z_b / \partial x}{\tan\varphi}.P$$

with:

(B6a) for $\alpha_b^2 u^2 > \tilde{U}^2$: $$P = \left\{\alpha_b^3\left|u^3\right| + \frac{3}{4}\alpha_b\hat{U}^2|u|\right\}$$ current dominant

(B6b) for $\tilde{U}^2 > \alpha_b^2 u^2$: $$P = \left\{\frac{4}{3\pi}\hat{U}^3 + \frac{3}{\pi}\alpha_b^2 u^2\hat{U}\right\}$$ wave dominant

The first parts of the bed-load expression are a pure current and a combined wave-current contribution (indicated respectively with superscripts ..^{c} and ..^{wc}):

(B7) $$q_b = q_b^c + q_b^{wc} - m_b \frac{\partial z_b / \partial x}{\tan\varphi}.P$$

(B7a) $$q_b^c = m_b\alpha_b^3 u^3$$

(B7b) $$q_b^{wc} = \frac{1}{2}m_b\alpha_b\hat{U}^2 u$$

The ‘ equilibrium’ suspended sediment load can be written, following Bailard (1981), as:

(B8) $$L = \overline{C}_e.h = m_s\left|u_s^3\right|$$

The ‘ equilibrium’ suspended transport rate as:

(B9) $$q_{s_e} = L.u_s = m_s\left|u_s^3\right|u_s$$

Similar to u_b, the near-bed intra-wave flow velocity u_s is composed of a near-bed horizontal orbital flow velocity (oscillatory flow with amplitude $\hat{U}$) and (normal to this) a near-bed steady flow velocity $\alpha_s u$ (u=depth-averaged velocity), with α_s a factor <1 which should be selected (standard α_s =0.5).
The derived approximated expressions (B4) and (B5) can also be used here with $\alpha_b = \alpha_s$.
Together with (B8) the following expressions result for *the depth-averaged ‘equilibrium’ sediment concentration* $\overline{C}_e$*:*

(B10a) for $\alpha_s^2 u^2 > \tilde{U}^2$: $$\overline{C}_e = \frac{m_s}{h}\left\{\alpha_s^3\left|u^3\right| + \frac{3}{4}\alpha_s\hat{U}^2|u|\right\}$$ current dominant

(B10b) for $\widetilde{U}^2 > \alpha_s^2 u^2$: $\overline{C}_e = \frac{m_s}{h}\left\{\frac{4}{3\pi}\hat{U}^3 + \frac{3}{\pi}\alpha_s^2 u^2 \hat{U}\right\}$ wave dominant

which can also be written as:

(B11a) for $\alpha_b^2 u^2 > \widetilde{U}^2$: $\overline{C}_e = \frac{m_s}{|q|}\left\{\alpha_s^3 u^4 + \frac{3}{4}\alpha_s \hat{U}^2 u^2\right\}$ current dominant

(B11b) for $\widetilde{U}^2 > \alpha_b^2 u^2$: $\overline{C}_e = \frac{m_s}{|q|}\left\{\frac{4}{3\pi}\hat{U}^3|u| + \frac{3}{\pi}\alpha_s^2|u^3|\hat{U}\right\}$ wave dominant

The equilibrium suspended transport in the direction of the steady current is now:

(B12) $q_s = q_s^c + q_s^{wc}$

with for $\alpha_b^2 u^2 > \widetilde{U}^2$:

(B12a) $q_s^c = m_s \alpha_s^4 |u^3| u$

$q_s^{cw} = \frac{3}{4} m_s \hat{U}^2 \alpha_s^2 |u| u$

and for $\widetilde{U}^2 > \alpha_b^2 u^2$:

(B12b) $q_s^c = 0$

$q_s^{wc} = m_s \alpha_s \hat{U}^3 |u| + m_s \alpha_s^3 \hat{U} |u^3|$

Appendix C Migration velocities and diffusion coefficients in the case of power-law type bed-load and suspended-load transport formulas

For the hyperbolic bed level model the following general expressions are derived for the migration velocities c_b and c_s and diffusion coefficients D_{i_b} and D_{i_s} expressed in terms of basic state parameters (see (23) and (24):

(C1) $$c_b = \frac{\mathrm{X}_1}{(1-\varepsilon_0)} = \frac{u_0[f_{1u}^{'}]_0}{(1-\varepsilon_0)h_0} - \frac{[f_3]_0 k_{w_\infty}[f_{1\hat{U}}^{'}]_0}{1-\varepsilon_0}$$

(C2) $$c_s = \frac{\alpha_s q \mathrm{X}_2}{(1-\varepsilon_0)} = \frac{u_0 \alpha_s q[f_{2u}^{'}]_0}{(1-\varepsilon_0)h_0} - \frac{\alpha_s q[f_3]_0 k_{w_\infty}[f_{2\hat{U}}^{'}]_0}{1-\varepsilon_0}$$

(C3) $$D_{i_b} = \frac{[f_{1\,i_b}^{'}]_0}{(1-\varepsilon_0)}$$

(C4) $$D_{i_s} = \frac{\alpha_s q[f_{2i_b}^{'}]_0}{(1-\varepsilon_0)}$$

The functions f_1, f_2 are specific for the power-law transport formula description for bed-load and suspended-load following the approach of Bailard (1981) (see Appendix B). Function f_3 is derived from linear wave theory in Appendix A.
The bed-load function f_1 can be written as:

(C5) $$q_b = f_1 = m_b\left[\ \alpha_b^3 u^3 + \frac{1}{2}\alpha_b u \hat{U}^2\ \right] - m_b \frac{i_b}{\tan\varphi}.P$$

with:

(C5a) for $\alpha_b^2 u^2 > \tilde{U}^2$: $$P = \left\{\alpha_b^3 |u^3| + \frac{3}{4}\alpha_b \hat{U}^2 |u|\right\}$$ current dominant

(C5b) for $\tilde{U}^2 > \alpha_b^2 u^2$: $$P = \left\{\frac{4}{3\pi}\hat{U}^3 + \frac{3}{\pi}\alpha_b^2 u^2 \hat{U}\right\}$$ wave dominant

Furthermore, for f_2:

(C6a) for $\alpha_b^2 u^2 > \tilde{U}^2$: $\overline{C}_e = f_2 = \frac{m_s}{|q|}\left\{\alpha_s^3 u^4 + \frac{3}{4}\alpha_s \hat{U}^2 u^2\right\}$ current dominant

(C6b) for $\tilde{U}^2 > \alpha_b^2 u^2$: $\overline{C}_e = f_2 = \frac{m_s}{|q|}\left\{\frac{4}{3\pi}\hat{U}^3|u| + \frac{3}{\pi}\alpha_s^2|u^3|\hat{U}\right\}$ wave dominant

and for f_3:

(C7)

$$f_3 = -\frac{\pi H}{T}\frac{\cosh k_w h}{(k_w h + \sinh(k_w h)\cosh(k_w h)).\tanh^2 k_w h}$$

Taking the derivatives as needed in (C1)...(C4):

(C8) $[f'_{1u}]_0 = \frac{3q^c_{b_0}}{u_0} + \frac{q^{wc}_{b_0}}{u_0}$ current- and wave dominant

(C9) $[f'_{1\hat{U}}]_0 = \frac{2q^{wc}_{b_0}}{\hat{U}_0}$ current- and wave dominant

(C10a) $[f'_{1i_b}]_0 = -\frac{1}{\tan\varphi}[|q^c_{b_0}| + \frac{3}{2}|q^{wc}_{b_0}|]$ current dominant

(C10b) $[f'_{1i_b}]_0 = -\frac{1}{\tan\varphi}[q^w_{b_0} + \frac{3}{2}q^{cw}_{b_0}]$ wave dominant

with:

(C11a) $q^c_{b_0} = m_b \alpha_b^3 u_0^3$ current dominant

(C11b) $q^{wc}_{b_0} = \frac{1}{2} m_b \alpha_b \hat{U}_0^2 u_0$

(C12a) $q^w_{b_0} = m_b \frac{4}{3\pi}\hat{U}^3$ wave dominant

(C12b) $q^{cw}_{b_0} = \frac{2}{\pi} m_b \alpha_b^2 \hat{U}_0 u_0^2$

and:

(C13a) $$[f_{2_u}^{'}]_0 = \frac{4q_{s_0}^{c}}{\alpha_s q u_0} + \frac{2q_{s_0}^{wc}}{\alpha_s q u_0}$$ current dominant

(C13b) $$[f_{2_u}^{'}]_0 = \frac{q_{s_0}^{w}}{\alpha_s q u_0} + \frac{3q_{s_0}^{cw}}{q u_0}$$ wave dominant

(C14a) $$[f_{2_{\hat{U}}}^{'}]_0 = \frac{2q_{s_0}^{wc}}{\alpha_s q \hat{U}_0}$$ current dominant

(C14b) $$[f_{2_{\hat{U}}}^{'}]_0 = \frac{3q_{s_0}^{w}}{\alpha_s q \hat{U}_0} + \frac{q_{s_0}^{cw}}{\hat{U} q}$$ wave dominant

(C15) $$[f_{2_{i_b}}^{'}]_0 = 0$$ current and wave dominant

with:

(C16a) $$q_{s_0}^{c} = m_s \alpha_s^4 u_0^4 \frac{q}{|q|}$$ current dominant

(C16b) $$q_{s_0}^{wc} = \frac{3}{4} m_s \alpha_s^2 \hat{U}_0^2 u_0^2 \frac{q}{|q|}$$

(C17a) $$q_{s_0}^{w} = m_s \frac{4}{3\pi} \hat{U}_0^3 \alpha_s u_0$$ wave dominant

(C17b) $$q_{s_0}^{cw} = \frac{3}{\pi} m_s \alpha_s^2 \hat{U}_0 u_0^3$$

The contribution of the waves in the current-dominated expressions is indicated with the superscript $..^{wc}$, while the contribution of the current in the wave-dominated expressions is indicated with $..^{cw}$.

Finally, the following expressions are found:

(C18) $$c_b = \frac{1}{(1-\varepsilon_0)h}[3q_{b_0}^{c} + q_{b_0}^{wc}(1+2f)]$$ current and wave dominant

(C19a) $$c_s = \frac{1}{(1-\varepsilon_0)h}[4q_{s_0}^{c} + 2q_{s_0}^{wc}(1+f)]$$ current dominant

(C19b) $$c_s = \frac{1}{(1-\varepsilon_0)h}[q_{s_0}^{w}(1+3f) + \alpha_s q_{s_0}^{cw}(3+f)]$$ wave dominant

(C20a) $$D_{i_b} = -\frac{\left|q_{b_0}^{c}\right| + \frac{3}{2}\left|q_{b_0}^{wc}\right|}{(1-\varepsilon_0)\tan\varphi}$$ current dominant

(C20b) $$D_{i_b} = -\frac{q_b^{w} + \frac{3}{2}q_b^{cw}}{(1-\varepsilon_0)\tan\varphi}$$ wave dominant

with:

(C21)

$$f = f(k_{w_0}h_0) = \frac{k_{w_\infty}h_0 \sinh k_{w_0}h_0 \cosh k_{w_0}h_0}{(k_{w_0}h_0 + \sinh k_{w_0}h_0 \cosh k_{w_0}h_0)\tanh^2 k_{w_0}h_0} = \frac{k_{w_\infty}h_0.\sinh(2k_{w_0}h_0)}{(2k_{w_0}h_0 + \sinh(2k_{w_0}h_0)).\tanh^2(k_{w_0}h_0)}$$

Appendix D Migration velocity and amplitude decay time for current and waves (wave dominated conditions)

Substituting of (38a,b) and (39c,d) into the full expression (45) gives:

(D1)

$$\widetilde{c}_{bed} = 1 + \frac{\frac{4}{3}\frac{\varepsilon_s}{\varepsilon_b}\tan\varphi\frac{\alpha_s^4}{\alpha_b^3}\frac{C}{\sqrt{g}}\frac{|u_{*0}|}{W_s}\frac{\hat{U}_0}{|u_0|}\left\{(1+3f)\left(\frac{\hat{U}_0}{u_0}\right)^2\frac{1}{3\pi\alpha_s^3}+(3+f)\frac{3}{4\pi\alpha_s}\right\}+\frac{1}{6}\frac{1}{\alpha_b^2}\left(\frac{\hat{U}_0}{u_0}\right)^2(1+2f)}{\widetilde{L}^2\frac{C^2}{g}\left(\frac{u_{*0}}{W_s}\right)^2 k^2 {h_0}^2+1}$$

with f according to (38c).

Using linear wave theory for $\hat{U}_0$ (3) and using $k_{w_\infty} = \frac{4\pi^2}{gT^2}$:

(D2)
$$\frac{\hat{U}_0}{u_0} = \frac{\pi H_0}{2Tu_0\sinh k_w h_0} = \frac{1}{2}\frac{H_0}{h_0}\frac{\sqrt{gh_0}}{u_0}\frac{\sqrt{k_{w_\infty}h_0}}{\sinh k_w h_0}$$

With $Fr = u_0/\sqrt{gh_0}$ substitution of D2 in D1 gives:

(D3)

$$\widetilde{c}_{bed} = 1 + \frac{1}{24}\frac{1}{\alpha_b^2}\frac{k_{w_\infty}h_0}{Fr^2}\left(\frac{H_0}{h_0}\right)^2\frac{(1+2f)}{\sinh^2 k_w h_0} + \widetilde{c}_s^{\,c}.\frac{\hat{U}_0}{u_0}\left[(1+3f)\frac{1}{12\pi}\frac{1}{\alpha_s^3}\frac{k_{w_\infty}h_0}{Fr^2}\left(\frac{H_0}{h_0}\right)^2\frac{1}{\sinh^2 k_w h_0}+(3+f)\frac{3}{4\pi\alpha_s}\right.$$

with:

(D3a)
$$\widetilde{c}_s^{\,c} = \frac{\frac{4}{3}\frac{\varepsilon_s}{\varepsilon_b}\tan\varphi\frac{\alpha_s^4}{\alpha_b^3}\frac{C}{\sqrt{g}}\frac{|u_{*0}|}{W_s}}{\widetilde{L}^2\frac{C^2}{g}\left(\frac{u_{*0}}{W_s}\right)^2 k^2 {h_0}^2+1}$$

(D3b)
$$f = \frac{k_{w_\infty} h_0 . \sinh(2k_w h_0)}{(2k_w h_0 + \sinh(2k_w h_0)) . \tanh^2(k_w h_0)}$$

Using (38), (39), (40) and (6a) in combination with (46) gives for the amplitude decay time in a similar way :

(D4)
$$\widetilde{T}_{bed} = \left\{ \frac{1}{\widetilde{T}_s^c} \frac{\hat{U}_0}{u_0} \left[(1+3f) \frac{1}{3\pi\alpha_s^3} \left(\frac{\hat{U}_0}{u_0} \right)^2 + \frac{(3+f)3}{4\pi\alpha_s} \right] + \frac{1}{\widetilde{T}_b^c} \frac{\hat{U}_0}{u_0} \left[\frac{4}{3\pi} \frac{1}{\alpha_b^3} \left(\frac{\hat{U}_0}{u_0} \right)^2 + \frac{3}{\pi\alpha_b} \right] \right\}^{-1}$$

or rewriting $\hat{U}_0 / u_0$ using D2 gives:

(D5)
$$\widetilde{T}_{bed} = \left\{ \frac{1}{\widetilde{T}_s^c} \frac{\hat{U}_0}{|u_0|} \left[(1+3f) \frac{1}{12\pi\alpha_s^3} \frac{k_{w_\infty} h_0}{Fr^2} \left(\frac{H_0}{h_0} \right)^2 \frac{1}{\sinh^2 k_w h_0} + \frac{3}{4\pi\alpha_s} (3+f) \right] + \right.$$
$$\left. + \frac{1}{\widetilde{T}_b^c} \frac{\hat{U}_0}{|u_0|} \left[\frac{1}{3\pi\alpha_b^3} \frac{k_{w_\infty} h_0}{Fr^2} \left(\frac{H_0}{h_0} \right)^2 \frac{1}{\sinh^2 k_w h_0} + \frac{3}{\pi\alpha_b} \right] \right\}^{-1}$$

with:

(D5a)
$$\widetilde{T}_s^{\,c} = \left\{ (kh_0)^2 \frac{\frac{4}{3} \widetilde{L} \frac{\varepsilon_s}{\varepsilon_b} \tan\varphi \frac{\alpha_s^4}{\alpha_b^3} \frac{C^2}{g} \left(\frac{u_{*_0}}{W_s} \right)^2}{1 + \widetilde{L}^2 \frac{C^2}{g} \left(\frac{u_{*_0}}{W_s} \right)^2 k^2 h_0^2} \right\}^{-1}$$

(D5b)
$$\widetilde{T}_b^{\,c} = \left\{ \frac{(kh_0)^2}{3\tan\varphi} \right\}^{-1}$$

Appendix E 1DH modelling of sand pit morphology in the marine environment: a numerical model

Ribberink, J.S. and R.H. Buijsrogge (2003)
Technical Note, EU project Sandpit, October 2003.

Abstract

A 1DH model is described for the morphodynamic behaviour of rectangular sand pits or channels under the influence of co-linear tidal flows normal to the main axis of the pit/channel and (non-breaking) short surface waves. The tidal flow is assumed to be frictionless with Froude numbers Fr<<1 , the short wave characteristics are spatially constant and linear wave theory is assumed to be valid for the description of the near-bed wave orbital flow. Sediment transport is described with the transportformula of Bailard (1981) for the bed-load transport and a depth-averaged model for suspended sediment, including spatial lag effects, based on Galappatti and Vreugdenhil (1985) and Bailard (1981). Measured sand pit morphodynamics during two laboratory cases with steady flow and one field case with tidal flow are well reproduced by the LOMOR model, provided a calibration factor α_{cal} for the sediment transport formula is used ($0.4< \alpha_{cal} <1$).

Problem schematization

Long sand pits are considered with their main axis normal to the direction of the co-linear tidal flow. The surrounding sea bed is assumed to be horizontal. In this way the morphological development of the pit is treated as a one-dimensional problem (x-direction is tidal flow direction).

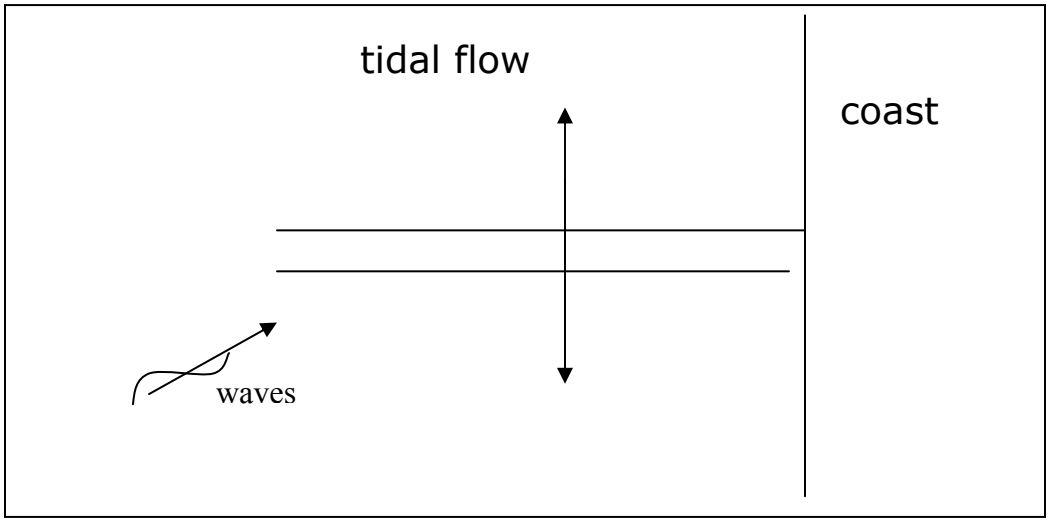

Figure 1 Sand pits normal to a co-linear tidal flow

Basic equations

Tidal flow

The one-dimensional shallow-water flow equations for depth-averaged flow are:

$$\frac{\partial u}{\partial t} + u\frac{\partial u}{\partial x} + g\frac{\partial z_b}{\partial x} + g\frac{\partial h}{\partial x} = R$$

$$\frac{\partial h}{\partial t} + \frac{\partial uh}{\partial x} = 0$$

with:

u = depth averaged flow velocity
h = water depth
z_b = bed level

Assuming co-linear tidal flow, short pit lenghts (<< tidal excursion length) and small Froude numbers (Fr<<1), the equations can be simplified to the following quasi-steady equations:

$$\frac{\partial z_b}{\partial x} + \frac{\partial h}{\partial x} = 0$$

$$\frac{\partial uh}{\partial x} = 0$$

Waves

Short wave characteristics wave height H and wave period T are assumed to be spatially constant and are not affected by the pit. Linear wave theory is assumed to be valid for the description of the near-bed wave orbital flow:

$$\hat{U}_{orb} = \pi\frac{H}{T}\frac{1}{\sinh(kh)}$$

k = wave number
h = water depth

Sediment transport
The bed-load transport is described with the formula of Bailard (1981). Only the current-related transport component, in the direction of the tidal flow, is taken into account. Wave-related transport is neglected and only the stirring influence of waves is included. Moreover, the formula contains the influence of (longitudinal) bed-slopes on the transport rate.

The near-bed intra-wave flow velocity u_b ,driving the sedimenttransport, is composed of a near-bed horizontal orbital flow velocity (oscillatory flow with amplitude $\hat{U}$) and, normal to this, a near-bed tidal flow velocity $\alpha_b u$ (u=depth-averaged velocity), with α_b a factor <1 which should be selected (standard α_b=0.5).
The bed-load formula of Bailard for the short-wave averaged bed-load transport can be written as:

$$q_b = m_b < u_b^2 > \alpha_b u - m_b \frac{\partial z_b / \partial x}{\tan\varphi} < \left| u_b^3 \right| >$$

with:

<..> = time-averaged over short-wave period

$$m_b = \frac{c_f \varepsilon_b}{\Delta g \tan\phi}$$

ε_b = 0.1 (efficiency factor)
c_f = wave friction factor (Swart, 1974)
Δ = relative sediment density
φ = angle of repose = 32 degr.

The velocity moments $<u_b^2>$ and $<|u_b^3|>$ are expressed in the near-bed tidal flow velocity $\alpha_b u$ and the near-bed wave orbital velocity amplitude $\hat{U}$ using simple analytical expressions (see Ribberink, 1989).

Suspended sediment concentrations are described with the depth-averaged formulation of Galappatti (1989), based on an asymptotic solution of the 3D advection-diffusion equation. In one-dimensional form:

$$T_A \frac{\partial \overline{C}}{\partial t} + L_A \frac{\partial \overline{C}}{\partial x} = \overline{C_e} - \overline{C}$$

With:
$\overline{C}$ = depth-averaged sediment concentration
T_A = adjustment time of suspended sediment

L_A = adjustment length of suspended sediment
$\overline{C_e}$ = depth-averaged equilibrium sediment concentration

For sand the adjustment time T_A (order of magnitude: h/Ws) is generally << tidal wave period T and a quasi-steady approach is justified:

$$L_A \frac{\partial \overline{C}}{\partial x} = \overline{C_e} - \overline{C}$$

The equilibrium concentration is based on the absolute magnitude of the third power of near-bed velocity u_s, according to formula of Bailard (1981) for suspended sediment. Similar to u_b, the near-bed intra-wave flow velocity u_s is composed of a near-bed horizontal orbital flow velocity (oscillatory flow with amplitude $\hat{U}$) and (normal to this) a near-bed tidal flow velocity $\alpha_s u$ (u=depth-averaged velocity), with α_s a factor <1 which should be selected (standard α_s =0.5).

$$\overline{C_e} = \frac{m_s}{h} < \left| \vec{u}_s^{\,3} \right| >$$

in which :

$$m_s = \frac{\varepsilon_s c_f}{\Delta g W_s}$$

ε_s = 0.02 (efficiency factor)
W_s= settling velocity of sediment

The adjustment length c an be written as:

$$L_A = \tilde{L}.\frac{u.h}{W_s}$$

With $\tilde{L}$ is a coefficient, which in principle depends on the shape of the vertical concentration distribution ($0.1 < \tilde{L} < 1$) . It is treated here as a constant which has to be selected in advance (standard value $\tilde{L}$ =0.5)
The suspended sediment transport can now be calculated from :

$$q_s = \alpha_s u h \overline{C}$$

Bed-level changes
The bed-level changes are calculated with the sediment continuity equation :

$$\frac{\partial z_b}{\partial t} + \frac{1}{1-\varepsilon_0}\frac{\partial \langle q_b + q_s \rangle}{\partial x} = 0$$

with:

ε_0 = porosity (=0.4)

Numerical model (LOMOR)

In the numerical model LOMOR the flow and sediment equations are solved according to the following flow scheme:

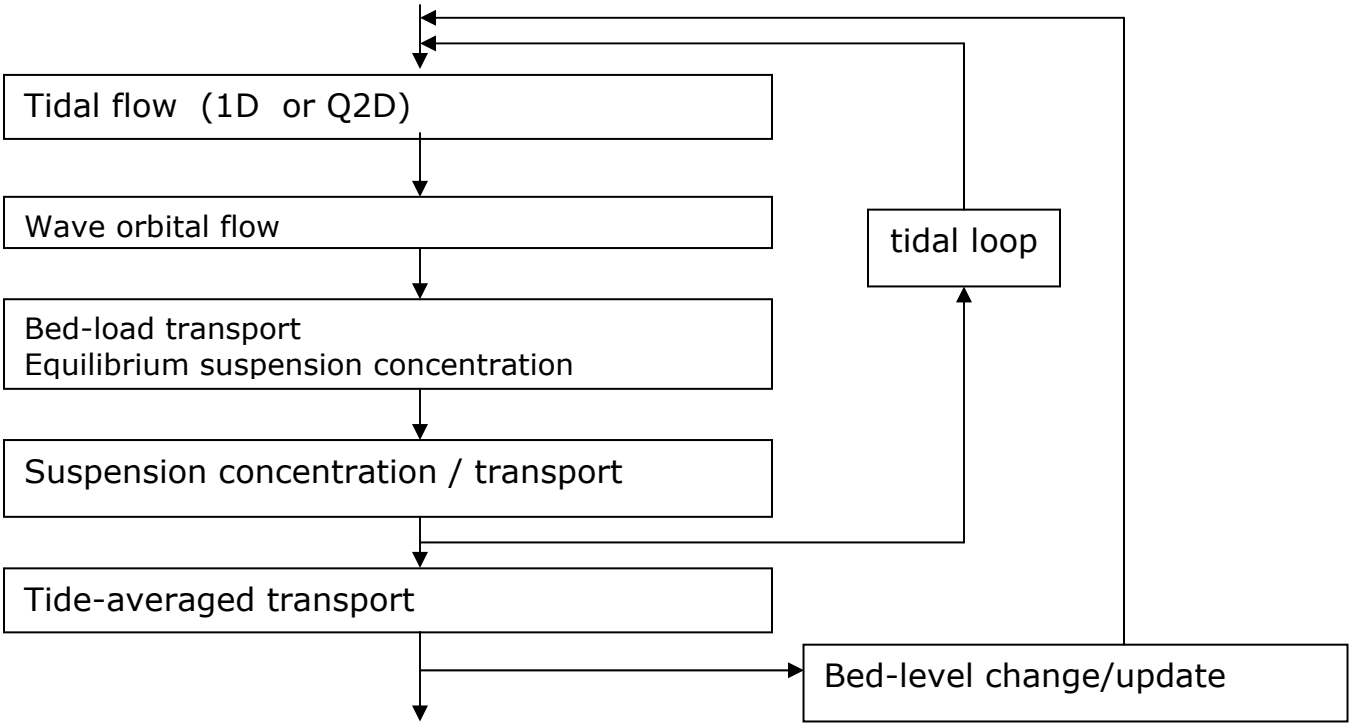

Figure 2 LOMOR flow chart

The equations are solved for successive time steps during a representative tide (time – series of u and h combinations above the local undisturbed sea bed, without sand pit). Tide-averaged sediment transport rates are used for updating the bed level. The morphological time-step can be one or more tidal periods. In the case local wave conditions are variable in time, a time series of wave conditions can be used as input for the model.

Benchmark pit computations

Two laboratory experiments and one field case are simulated by the LOMOR model. The lab cases are a wave basin experiment (Case I) and a flume experiment (Case II) with a steady current and constant wave conditions over a fine sand bed with an initial sand pit (see Sandpit WEB site)

	Case I	Case II
u (m/s)	0.245	0.18
h (m/s)	0.42	0.26
H (m)	0.105	0.08
T (s)	2.16	1.5
W_s (m/s)	0.006	0.007
Pit lenght (m)	4	4.5
Pit depth (m)	0.2	0.12
roughness height k_w (m)	0.01	0.035
α_{cal} (calibration factor)	0.94	0.45

Benchmark case III is a 45 m long and 3.5 m deep sand pit, which was excavated in the North Sea at a depth of ca. 8 m near Scheveningen (Dutch coast). The pit axis is oriented approximately normal to the tidal flow. A time-series of wave characteristics is available, representing the local wave conditions in the period after the pit was dredged. A representative vertical and horizontal (morphological) tide is used as input for the flow calculations. For more details about the Scheveningen pit, see Sandpit WEB-site.

For the laboratory cases I and II the LOMOR model is calibrated with a multiplication factor α_{cal} for the sediment transport (bed-load and suspended-load), using the measured suspended transport rates at the upstream boundary. The obtained calibration factors do not deviate too much from unity, for Case I: α_{cal}=0.97 and for Case II: α_{cal}=0.45.
The field case III was simulated with the uncalibrated model, since no transport measurements were available.
The computational results are shown in the figures below .

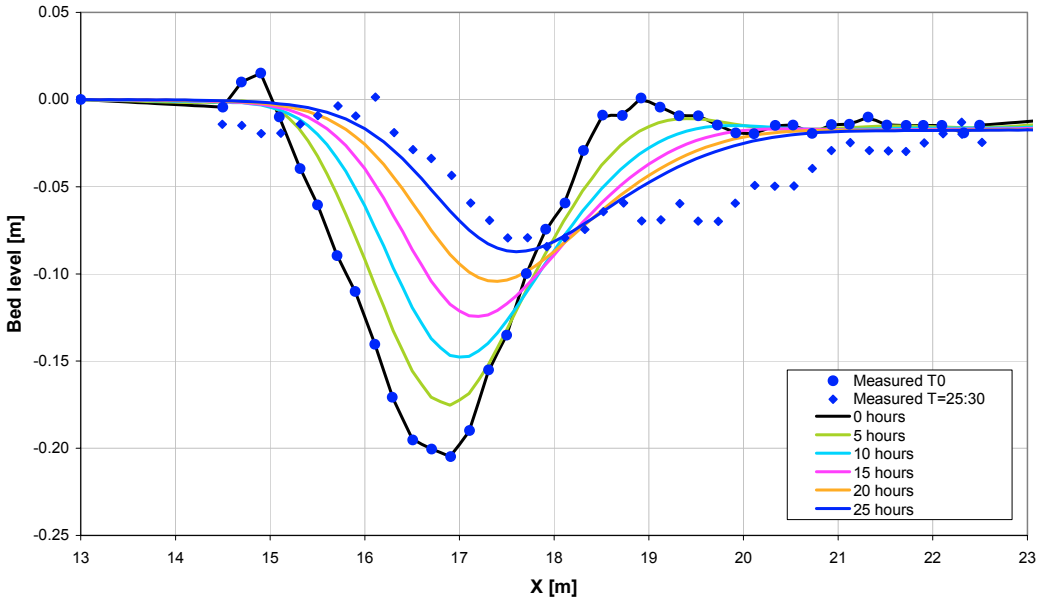

Figure 3 Case I: laboratory flume experiment

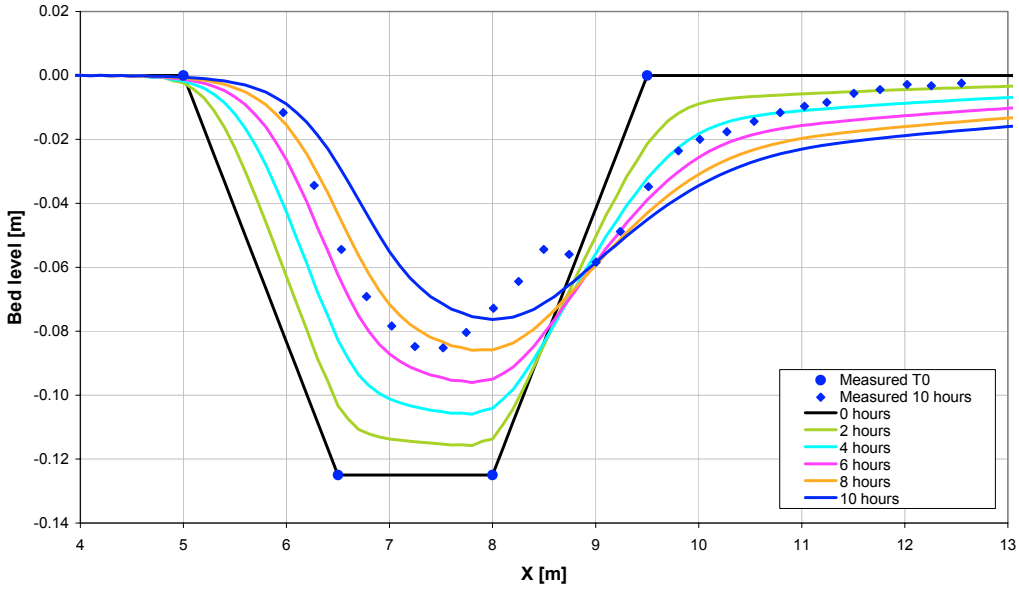

Figure 4 Case II: Laboratory basin experiment

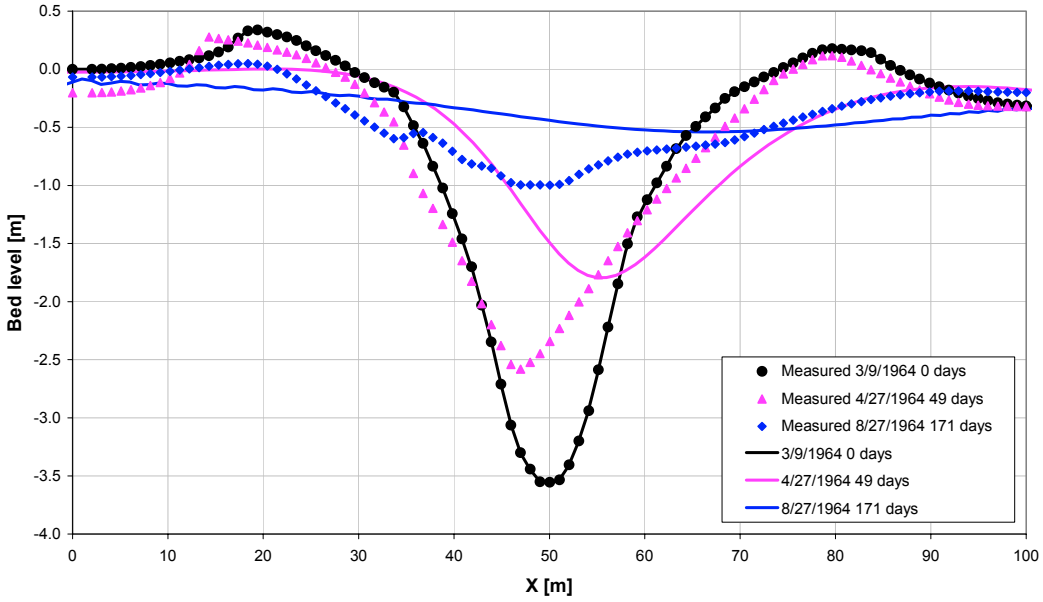

Figure 5 Case III: Scheveningen sand pit in the North Sea

The lab cases are simulated in a reasonable way by the LOMOR model. The migration speed of the pit is slightly underestimated or overestimated for respectively the cases I and II. The sedimentation rate of the pit (damping) is reasonably described in both cases. The morphological time scale of the Scheveningen pit development is overestimated by the (uncalibrated) model. Using a similar calibration (reduction) factor as for the Cases I and II provides a much better description of the time scale. The simulated migration of the pit is in positive x-direction, while the measurements show a small migration in the opposite direction.

References

Bailard, J.A. (1981), An energetics total load sediment transport model for a plane sloping beach, J. of Geoph. Res., Vol. 86, No. C11, November.

Galappatti, R. and C.B. Vreugdenhil (1985), A depth-integrated model for suspended transport, J. of Hydr. Res., Vol. 23, No. 4.

Ribberink, J.S. (1989), Zeezandwinning, onderbouwend rapport : milieu effect rapportage RON, discussienota kustverdediging , Technisch Rapport 10, Waterloopkundig Laboratorium, WL, H825 (in Dutch)

Swart, D.H. (1974), Offshore sediment transport and equilibrium beach profiles, Delft Hydr. Lab. Publ., No. 131, Delft Hydraulics, the Netherlands.